Impaired Myocardium Regeneration With Skeletal Cell Sheets—A Preclinical Trial for Tissue-Engineered Regeneration Therapy

Shigeru Miyagawa,[1] Atsuhiro Saito,[2] Taichi Sakaguchi,[1] Yasushi Yoshikawa,[1] Takashi Yamauchi,[1] Yukiko Imanishi,[1] Naomasa Kawaguchi,[3] Noboru Teramoto,[4] Nariaki Matsuura,[3] Hidehiro Iida,[4] Tatsuya Shimizu,[5] Teruo Okano,[5] and Yoshiki Sawa[1,6]

Background. We hypothesized that autologous skeletal cell (SC) sheets regenerate the infract myocardium in porcine heart as a preclinical trial.

Methods and Results. The impaired heart was created by implantation of ameroid constrictor on left anterior descending for 4 weeks. SCs isolated from leg muscle were cultured and detached from the temperature-responsive domain-coated dishes as single monolayer cell sheet at 20°C. The following therapies were conducted: SC sheets (SC group, n=5); sham (C group n=5). Echocardiography demonstrated that cardiac performance was significantly improved in the SC group 3 and 6 months after operation (fractional area shortening, 3 months; SC vs. C=49.5±2.8 vs. 24.6±2.0%, $P<0.05$) and left ventricle dilatation was well attenuated in the SC group. Color kinesis index showed that distressed regional diastolic and systolic function in infarcted anterior wall was significantly recovered (SC vs. C=57.4±8.6 vs. 30.2±4.7%, $P<0.05$, diastolic: 58.5±4.5 vs. 35.4±6.6%, $P<0.05$, systolic). Factor VIII immunostains demonstrated that vascular density was significantly higher in the SC group than the C group. And % fibrosis and cell diameter were significantly lower in the SC group. And hematoxylin-eosin staining depicted that skeletal origin cells and well-developed-layered smooth muscle cells were detected in the implanted area. Positron emission tomography showed better myocardial perfusion and more viable myocardial tissue in the distressed myocardium receiving SC sheets compared with the myocardium receiving no sheets.

Conclusions. SC sheet implantation improved cardiac function by attenuating the cardiac remodeling in the porcine ischemic myocardium, suggesting a promising strategy for myocardial regeneration therapy in the impaired myocardium.

Keywords: Cells, Heart failure, Myocardial infarction, Tissue, Transplantation.

(*Transplantation* 2010;90: 364–372)

Despite the recent remarkable progress in medical and surgical treatments for heart failure, end-stage heart failure has been still a major cause of death worldwide. After myocardial infarction, the myocardium is capable of a limited regenerative capacity and no medication or procedure used clinically has shown efficacy in regenerating myocardial scar tissue with functioning tissue. Thus, there is a need for new therapeutics to regenerate damaged myocardium.

Recent developments in tissue engineering show promise for the creation of functional cardiac tissues without the need for biodegradable alternatives for the extracellular matrix (*1*). And we reported that cardiomyocyte sheets have been developed by using temperature-responsive culture dishes and these sheets survived in the back of nude rats and showed a spontaneous contraction over a long period of time (*2*). Recent reports suggested that cardiomyocyte sheets integrated with the impaired myocardium and improved cardiac performance in a rat model of ischemic myocardium (*3*).

This work was supported by a Grant-in-Aid for Scientific Research in Japan.

[1] Division of Cardiovascular Surgery, Department of Surgery, Faculty of Medicine, Osaka University Graduate School of Medicine, Suita, Osaka, Japan.

[2] Medical Center for Translational Research, Osaka University Hospital, Osaka, Japan.

[3] Department of Pathology, School of Allied Health Science, Faculty of Medicine, Osaka University Graduate School of Medicine, Suita, Osaka, Japan.

[4] Department of Investigative Radiology, National Cardiovascular Center Research Institute, Tokyo, Japan.

[5] Tokyo Women's Medical University Institute of Advanced Biomedical Engineering and Science, Tokyo, Japan.

[6] Address correspondence to: Yoshiki Sawa, M.D., Department of Cardiovascular Surgery, Osaka University Graduate School of Medicine, 2-2 Yamada-oka, Suita, Osaka 565-0871, Japan.

E-mail: sawa@surg1.med.osaka-u.ac.jp

S.M. participated in the writing of the paper; A.S. participated in research design; T.S. and Y.Y. participated in data analysis; T.Y., Y.I., N.K., and N.T. participated in the performance of research; N.M., H.I., T.S., T.O., and Y.S. participated in research design.

Received 15 December 2009. Revision requested 2 January 2010.

Accepted 6 May 2010.

ISSN 0041-1337/10/9004-364

DOI: 10.1097/TP.0b013e3181e6f201

And more recently, in the aim of clinical application, nonligature implantation of skeletal myoblast sheet regenerated the damaged myocardium and improved global cardiac function by attenuating the cardiac remodeling in the rat ligation model (*4*) and dilated cardiomyopathy hamster model (*5*). This cell delivery system by using cell sheets implantation showed better restoration of damaged myocardium compared with needle injection (*4, 5*). Moreover, grafting of skeletal myoblast sheets attenuated cardiac remodeling and improved cardiac performance in pacing-induced canine heart failure model (*6*).

Given this body of evidence, we hypothesized that the autologous skeletal cell (SC) sheet implantation might remodel the chronic heart failure caused by ischemic injury.

Therefore, this preclinical study using Swine model was designed to test therapeutic effectiveness.

MATERIALS AND METHODS

Myocardial Infarction Model

"Principles of Laboratory Animal Care" formulated by the National Society for Medical Research and the "Guide for the Care and Use of Laboratory Animals" prepared by the Institute of Laboratory Animal Resource and published by the National Institutes of Health (NIH Publication No. 86-23, revised 1985). This animal experiment was approved by the Animal Care Committee of Osaka university graduate school of medicine. We induced acute myocardial infarction of 10 swine (20 kg, KEARI, Japan) by the following method. Swine were preanesthetized by intramuscular injection of ketamine hydrochloride 20 mg/kg (Ketalar, Sankyo, Japan) and xylazine 2 mg/kg (Seractar, Bayer). Animals were positioned spine and a 22-gauge indwelling needle (Surflo F&F, Terumo, Tokyo, Japan) was inserted in the central vein of the auricle. A three-way cock (Terufusion TS-TR2K, Terumo, Tokyo, Japan) was attached to the external cylinder of the indwelling needle, and an extension tube was connected for continuous anesthetic injection. The animals were intubated with an endotracheal cannula (6 Fr, Sheridan) using a pharyngoscope and then connected to an artificial respirator (Harvard, USA) by the cannula. Artificial respiration was implemented at a stroke volume of 200 to 300 mL/stroke and a stroke frequency of 20/min. The animals were continuously drip injected with propofol 6 mg/kg/hr (Diprivan, AstraZeneca) and vecuronium bromide 0.05 mg/kg/hr (Musculux, Sankyo Yell Yakuhin Co., Ltd., Japan) using a syringe pump (Terufusion TE-3310N, Terumo, Japan). The animal was then fixed in a recumbent position, so that the left thorax was exposed, and the outer layer of skin and muscles between the third and fourth ribs were dissected. After confirming the cutting into the thoracic cavity, the distance between the third and fourth ribs was widened with a rib spreader to allow a direct view of the left auricle and the LAD coronary artery. The pericardium was dissected along the LAD from the upper part of the left auricle (~6 cm) to expose the myocardium around the LAD. LAD on the proximal side below the left auricle from the myocardium was exfoliated for approximately 1 cm, and then a small amount of lidocaine hydrochloride jelly (Xylocaine jelly, AstraZeneca) was applied to allow for anesthetizing the area. An ameroid constrictor (COR-2.50-SS, Research Instruments) was then fit using No. 1 or 2 suture. The chest cavity was closed to end the procedures. The animals were randomly divided into two treatment groups: the first received autologous SC sheet implantation (SC group, n=5). For control, we have performed sham operation (C group, n=5).

Preparation of Skeletal Cell Sheets for Grafting

One week after implantation of ameroid constrictor on LAD, skeletal muscle weighing approximately 5 g was removed from the pretibial region with the porcine under general anesthesia. Following the addition of trypsin-ethylenediaminetetraacetic acid (Gibco, Grand Island, NY), excessive connective tissue was carefully removed to minimize the content of contaminating fibroblasts, and the muscle tissue was minced until the fine pieces formed a homogeneous mass. The specimens were then incubated at 37°C in shaker bath with 0.5% type 1 collagenase (Gibco) in Dulbecco's modified Eagle's medium (Gibco). After brief placement, the fluid was collected, and the same volume of culture medium, SkBM (Cambrex, Walkersville, MD) supplemented with fetal bovine serum (Thermo Trace, Melbourne, Australia), was added to halt the enzymatic digestion process. The cells were collected by centrifugation, and the putative SCs were seeded into 150 cm^2 polystyrene flasks after removal of fibroblasts by sedimentation for a few hours and cultured in SkBM at 37°C. During the culture process, we maintained cell densities at less than 70% confluence by carrying out passaging of cells for one time to prevent SCs from premature differentiation and fusion process resulting in myotubes formation. When the cells become approximately 70% confluent after 10 to 11 days cultivation, the cells were dissociated from the flasks with trypsin-ethylenediaminetetraacetic acid and reincubated on 100 mm temperature-responsive culture dishes (Cellseed, Tokyo, Japan) at 37°C with the cell numbers adjusted to 1×10^7 per dish. More than 90% of these cells were desmin positive (Fig. 1). After 4 days, the dishes were removed to refrigerator set at 20°C, and left there for approximately 30 min. During that time, the SC sheets detached spontaneously from the surfaces. Each sheet had a diameter of 30 to 40 mm and consisted of layers of SCs; the sheets were approximately 100-μm thick in cross-sectional views (Fig. 1). Approximately 10 sheets were obtained from the 5 g of skeletal muscle.

Implantation of Skeletal Cell Sheets

Autologous SC sheet implantation was performed in the swine 4 weeks after LAD ligation. Swine were anesthetized as mentioned above. The swine were exposed through the sternum. The infarct area was identified visually on the basis of surface scarring and abnormal wall motion. In the SC group, we implanted 10 SC sheets into the infarcted myocardium. The control group was treated similarly but received no SC sheets. Because pilling up four or more sheets caused the central necrosis of the myoblasts presumably because the lack of in oxygen supply, we decided to pile two or three layers of the SC sheet over the broad surface of the impaired heart.

Measurement of Cardiac Function

Swine were anesthetized as mentioned above. Cardiac ultrasonography was performed with a commercially available echocardiograph, SONOS 5500 (PHILIPS Electronics, Tokyo, Japan). A 3-MHz annular array transducer was placed on a layer of acoustic coupling gel that was applied to the left hemithorax. Swine were examined in a shallow left lateral decubitus position. The heart was first imaged in the two-dimensional mode in short-axis views at the level of the largest left ventricle (LV) diameter. The calculation of the LV volume was based on the LV short-axis area using AQ system (*7*). And fractional area shortening (FAS) of the LV diastolic was calculated as follows:

$$\text{FAS}\ (\%) = [(\text{LVend-diastolic area} - \text{LV end-systolic area [ESA]})/\text{LV end-diastolic area}] \times 100$$

These data are presented as the average of measurements of two or three selected beats.

Quantification of Regional Diastolic and Systolic Function by Color Kinesis

Diastolic CK images were obtained using a commercially available ultrasound system (SONOS 5500, Philips Medical Systems) from the LV midpapillary short-axis view for the determination of wall motion asynchrony as previously reported (*8*). CK examined every image pixel within the region of interest, which was drawn around the LV cavity, classifying it as blood or tissue based on integrated backscatter data. During diastole, each pixel was tracked into the next frame, and pixel transitions from endocardium to blood were detected and interpreted as diastolic endocardial motions. These pixel transitions were encoded using a color hue specific to each consecutive video frame, so that each color represents the excursion of that segment during a 33-ms period of time. The sites of regional LV diastolic wall motion or regions of interest were set on the basis of standard segmentation models: anterior, lateral, posterior, inferior, anteroseptal wall. The CK diastolic index was defined as the LV segmental filling fraction

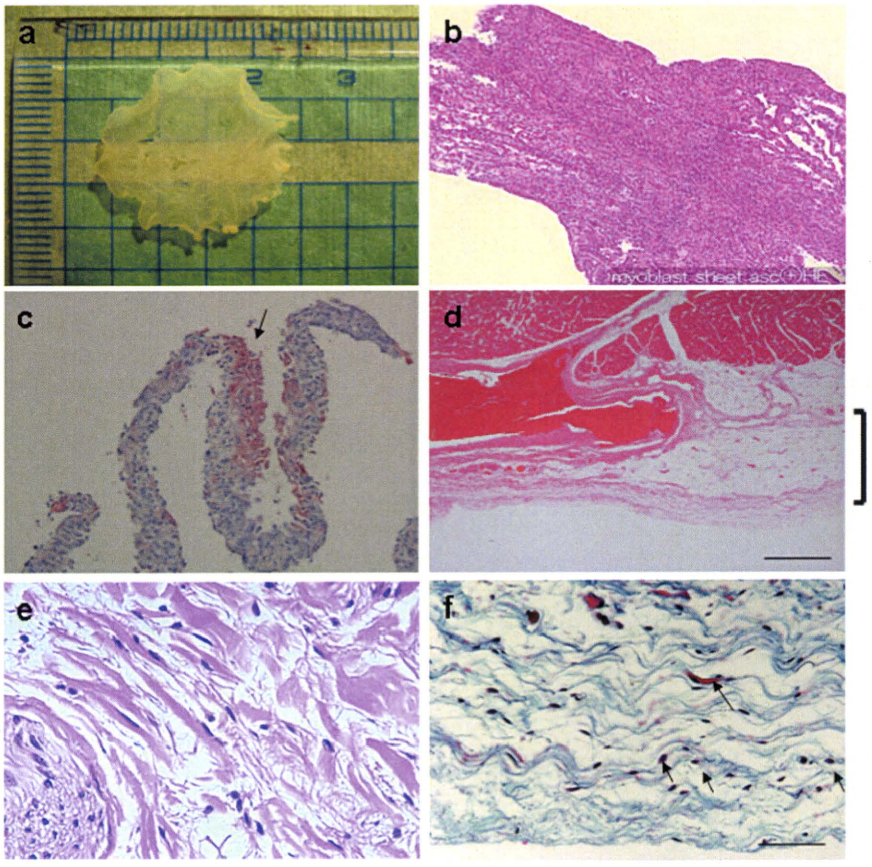

FIGURE 1. Histological characteristics of skeletal cell (SC) sheet. (a) SC sheet detached from the Poly (*N*-isopropylacrylamide)-grafted polystyrene by lowering the temperature. Its size is approximately 3 cm×2 cm^2. (b) Hematoxylin-eosin (H&E) stain; cross-sectional views of SC sheet in vitro. SC sheet demonstrates homogeneous heart-like tissue. (c) Not so many smooth muscle cells were detected in the SC sheets. The *arrow* indicates the smooth muscle cells in the SC sheet. (d) H&E stain revealed that SC sheets attached on the surface of epicardium. *Left square bracket* indicates implanted SC sheets. (e) Oval-shaped cells that showed positive for eosin in cytoplasm were detected in the SC group microscopically in some layers over epicardium. (f) Elastica Masson Goldner showed that oval-shaped cells that supposed to origin from skeletal tissue exist in the transplantation site. *Arrows* indicate oval-shaped cells that suppose to be originated form skeletal tissue.

during the first 30% of the diastolic filling time (LV segmental cavity area expansion during the first 30% of diastole, divided by the segmental end-diastolic LV cavity area expansion, expressed as a percentage). We introduced the use of color kinesis method that displays endocardial motion in real time to evaluate the regional systolic function (*8*).

Histopathology

LV myocardium specimens were obtained 6 months after the SC sheet implantation. Each specimen was fixed with 10% buffered formalin and embedded in paraffin. A few serial sections were prepared from each specimen and stained with hematoxylin-eosin (H&E) stain and elastica Masson-Goldner for histological examination or with Masson's trichrome stain to assess the collagen content.

To label vascular endothelial cells so that the blood vessels could be counted, immunohistochemical staining of factor VIII-related antigen was performed according to a modified protocol. Frozen sections were fixed with a 2% paraformaldehyde solution in phosphate-buffered saline (PBS) for 5 min at room temperature, immersed in methanol with 3% hydrogen peroxide for 15 min, then washed with PBS. The samples were covered with bovine serum albumin solution (DAKO LSAB Kit DAKO CORPORATION, Denmark) for 10 min to block nonspecific reactions. The specimens were incubated overnight with an Enhanced Polymer One-Step Staining (EPOS)-conjugated antibody against factor VIII-related antigen coupled with horseradish peroxidase (DAKO EPOS Anti-Human Von Wille brand Factor/HRP, DAKO, Denmark). After the samples were washed with PBS, they were immersed in diaminobenzidine solution (0.3 mg/mL diaminobenzidine in PBS) to obtain positive staining. Ten different fields at 200× magnification were randomly selected, and the number of the stained vascular endothelial cells in each field was counted under a light microscope. The result was expressed as the number of blood vessels per square millimeter.

The following antibodies against smooth muscle cells and skeletal myosin (slow) were used to evaluate the existence of SCs: primary antibodies, anti-smooth muscle actin (clone 1A4, DAKO) antiskeletal myosin (slow) (clone NOQ7.5.4D, Sigma); secondary antibodies, anti-mouse Ig biotinylate (DAKO).

Picro-sirius red staining for the assessment of myocardial fibrosis or periodic acid-Schiff staining for that of cardiomyocyte hypertrophy was performed as described (*9*).

Positron Emission Tomography Procedure

We performed positron emission tomography (PET) studies on pigs which were transplanted SC sheets and control by using ^{15}0-water and ^{18}F-FDG. The pigs were anesthetized by the introduction of pentobarbital followed by continuous inhalation of propofol (4 mg/kg/hr) and were placed supine on the bed of the scanner. PET was performed using a HEADTOME-III tomograph (Shimadzu, Kyoto, Japan) and data were analyzed as described elsewhere (*10*).

Holter Electrocardiography

To evaluate arrhythmia we used Holter electrocardiography (ECG) for 24 hours. We checked arrhythmia by checking the number of ventricular premature beat after SC sheet implantation in myocardial infarction porcine (n=3).

Data Analysis

Data are expressed as means ± SEM and subjected to multiple analysis of variance (ANOVA) using the StatView 5.0 program (Abacus Concepts, Berkeley, CA). Echocardiographic data were first analyzed by two-way repeated measurement ANOVA for differences across the whole time course, and one-way ANOVA with the Tukey-Kramer posthoc test was used to verify the significant for the specific comparison at each time point. To assess the significance of the differences between individual groups concerning other numeral data, statistical evaluation was performed with an unpaired *t* test. Statistical significance was determined as having a *P* value less than 0.05.

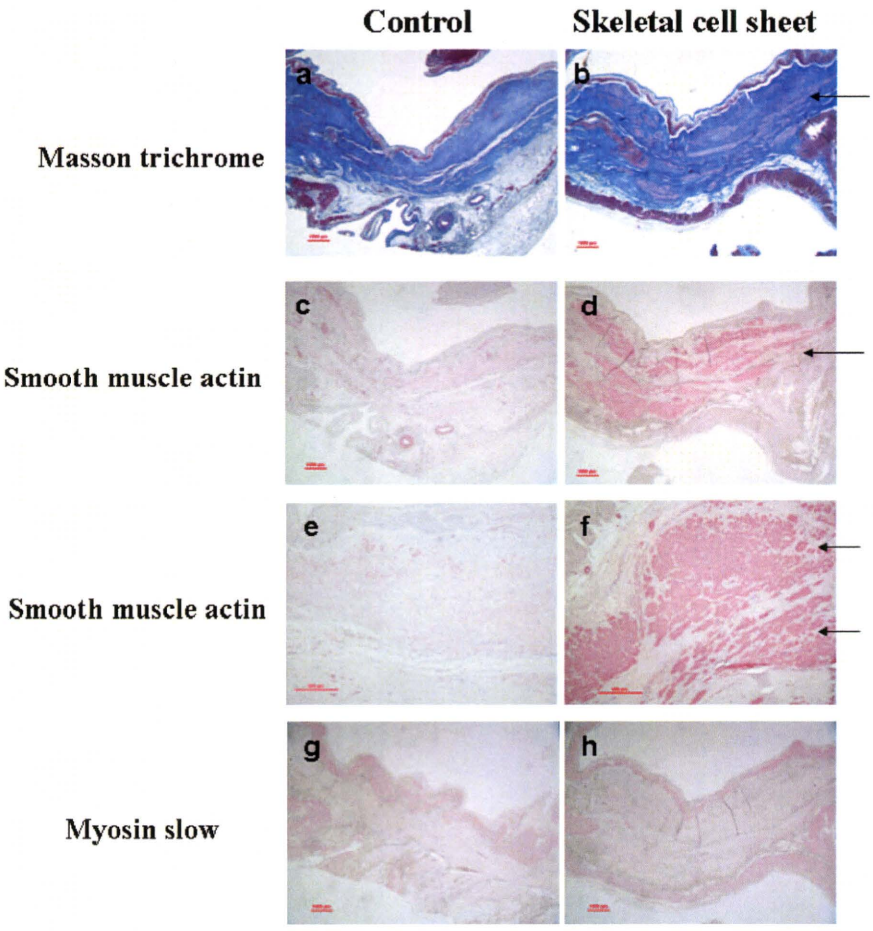

FIGURE 2. The detection of a large quantity of skeletal cells (SCs) in the center of the scar. (a and b) Masson trichrome staining reveals that some layered muscles are detected in the center of the scar in the SC sheet transplantation group, whereas not in the control. (c–f) Smooth muscle actin staining demonstrated that well-developed smooth muscle cells occupied in the center of the scar in the SC sheet transplantation group, whereas only smooth muscle cells which are formed vasculature are detected in the control. (g and h) Slow-type myosin staining showed that no positive cells exist in the center of the scar. This means that SCs which are detected in the center of the scar are not the residual myocyte after infarction.

RESULTS

Characteristics of Myoblast Sheet

We obtained monolayered myoblast sheets by lowering the temperature, which released them from the Poly(*N*-isopropylacrylamide)-grafted polystyrene. Its size is approximately 3 cm×2 cm^2 (Fig. 1a). H&E staining demonstrated that SC sheet contained a lot of SCs and SC sheets had an appearance of homogenous tissue, which thickness of one SC sheet was approximately 100 μm (Fig. 1b). Some smooth muscle cells are detected in the SC sheets, but those cells are not majority (Fig. 1c).

Histological Assessment

H&E staining demonstrated that transplanted SC sheets were attached in the epicardium (Fig. 1d) and oval-shaped cell that showed positive for eosin in cytoplasm were detected in the SC group microscopically in some layers over epicardium (Fig. 1e). Elastica Masson-Goldner showed that oval-shaped cells that supposed to origin from skeletal tissue exist in the transplantation site (Fig. 1f). These cells were not seen in the control group. And the SC group demonstrated decrease in the cross-sectional LV area compared with the C groups (Fig. 2a). Masson's trichrome staining showed that clustered SCs were detected in the center of the scar, whereas clustered SCs were not detected in the C group (Fig. 2a, b). Many clusters of well-developed smooth muscle cells exist in the center of the whole scar in the SC group, whereas in the C group, smooth muscle cells which formed vasculature exist in the scar (Fig. 2c–f). Although slow-type myosin-positive cells exist only on the endocardium and epicardium, those cells were not detected in the center of scar (Fig. 2g,h). So these figures depict that the skeletal muscle cells that exist in the center of the scar is not residual myocyte after infarction.

Quantification of Histopathology

In the SC group, vascular density was found to be significantly higher than in the C groups (SC vs. C=217.1±30.2 vs. 114.2±18.2 /field; $P<0.05$) (Fig. 3b).

Picro-sirius red staining demonstrated that % fibrosis was significantly reduced in the SC group compared with the C group (SC vs. C=1.6±0.2 vs. 3.1±0.3%; $P<0.05$) (Fig. 3b). Periodic acid-Schiff staining showed that cell diameter was significantly shorter in the SC group than the C group (SC vs. C=10.7±0.3 vs. 18.3±1.4 μm; $P<0.05$) (Fig. 3b).

These histological findings were universally identified in the native myocardial tissue without distinction of distance from the grafted region.

Functional Assessment of the Infarcted Myocardium

The FAS and LV end-ESA scores at baseline were not significantly different between the two groups.

Three months after the implantation, two-dimensional echocardiography showed significant improvement of the

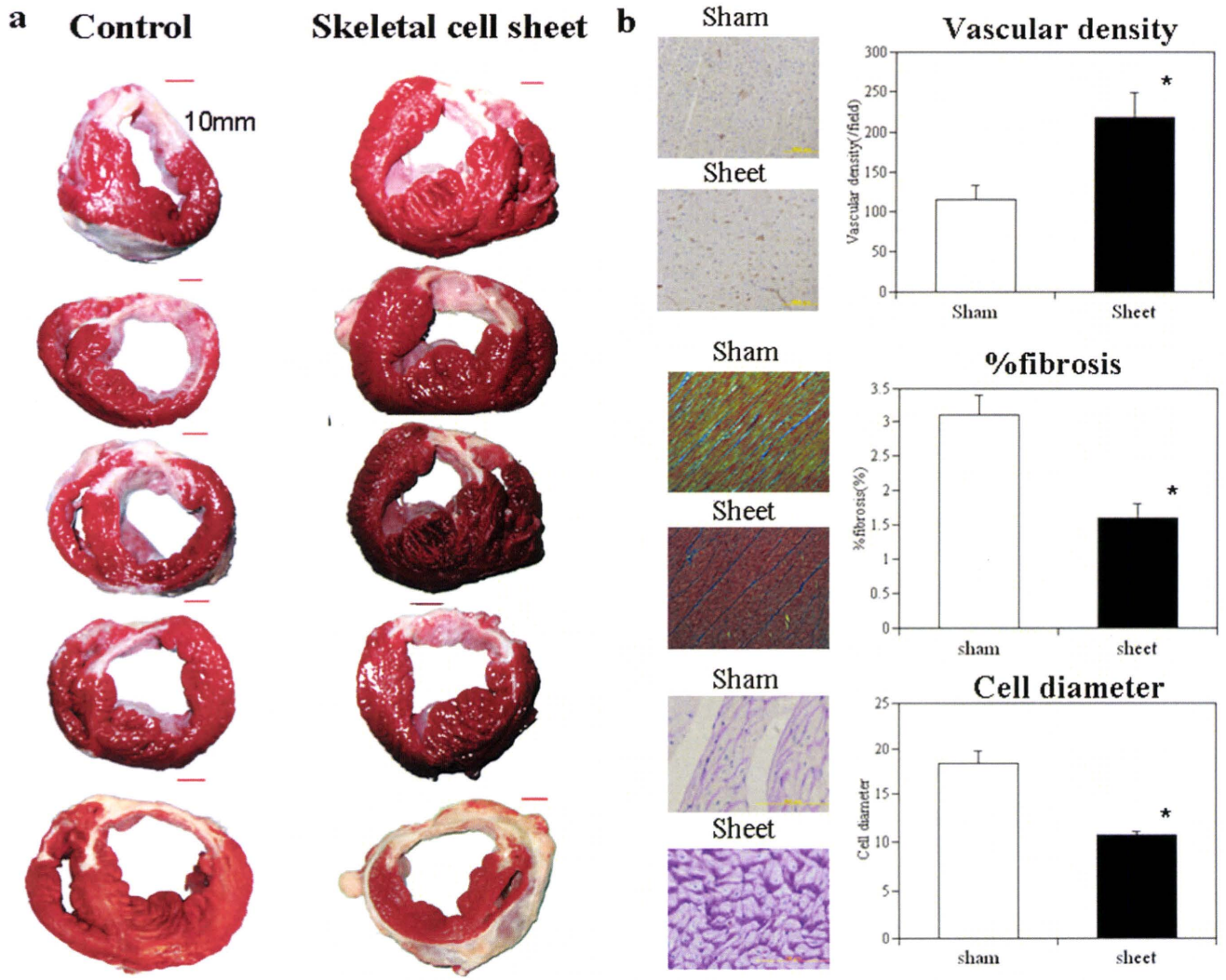

FIGURE 3. Macroscopic images of impaired myocardium receiving skeletal cell (SC) sheets and histological evaluation. (a) In the SC group, the anterior wall has recovered compared with the C group. In the SC group, the short axis area of the left ventricle (LV) is small compared with the C groups. In contrast, the C group shows a dilated LV and the anterior wall is thinner than in the SC groups. (b) Histological evaluation. Vascular density: the SC group showed a significant improvement in vascular density as assessed by immunostaining for the factor VIII-related antigen. **P* less than 0.05 vs. C. The ratio of fibrosis-occupied area (% fibrosis) at a site remote from the infarcted heart region: picro-sirius red staining demonstrated that % fibrosis at a site remote from the infarcted heart region was significantly reduced in the SC group compared with the C group. **P* less than 0.05 vs. C. The diameter of cardiomyocyte: the diameter of cardiomyocyte is significantly shorter in the SC group than the C group. **P* less than 0.05 vs. C.

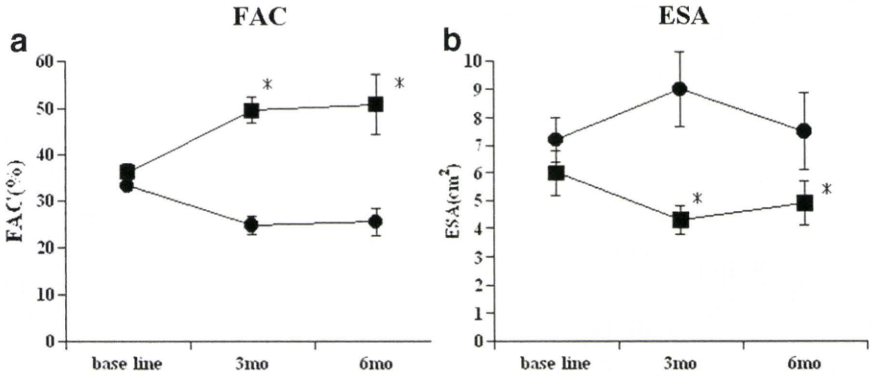

FIGURE 4. Global functional effects of infarcted myocardium receiving the implant. Global systolic function assessed by the fractional area shortening (FAS) (a) was significantly improved in the skeletal cell (SC) group 3 months after transplantation, and these functional improvements were preserved 6 months after SC sheet implantation. (b) The end-systolic area (ESA) was significantly smaller in the SC group than in the C groups 3 and 6 months after implantation. **P* less than 0.05 vs. C, ■: SC sheet, ●: control.

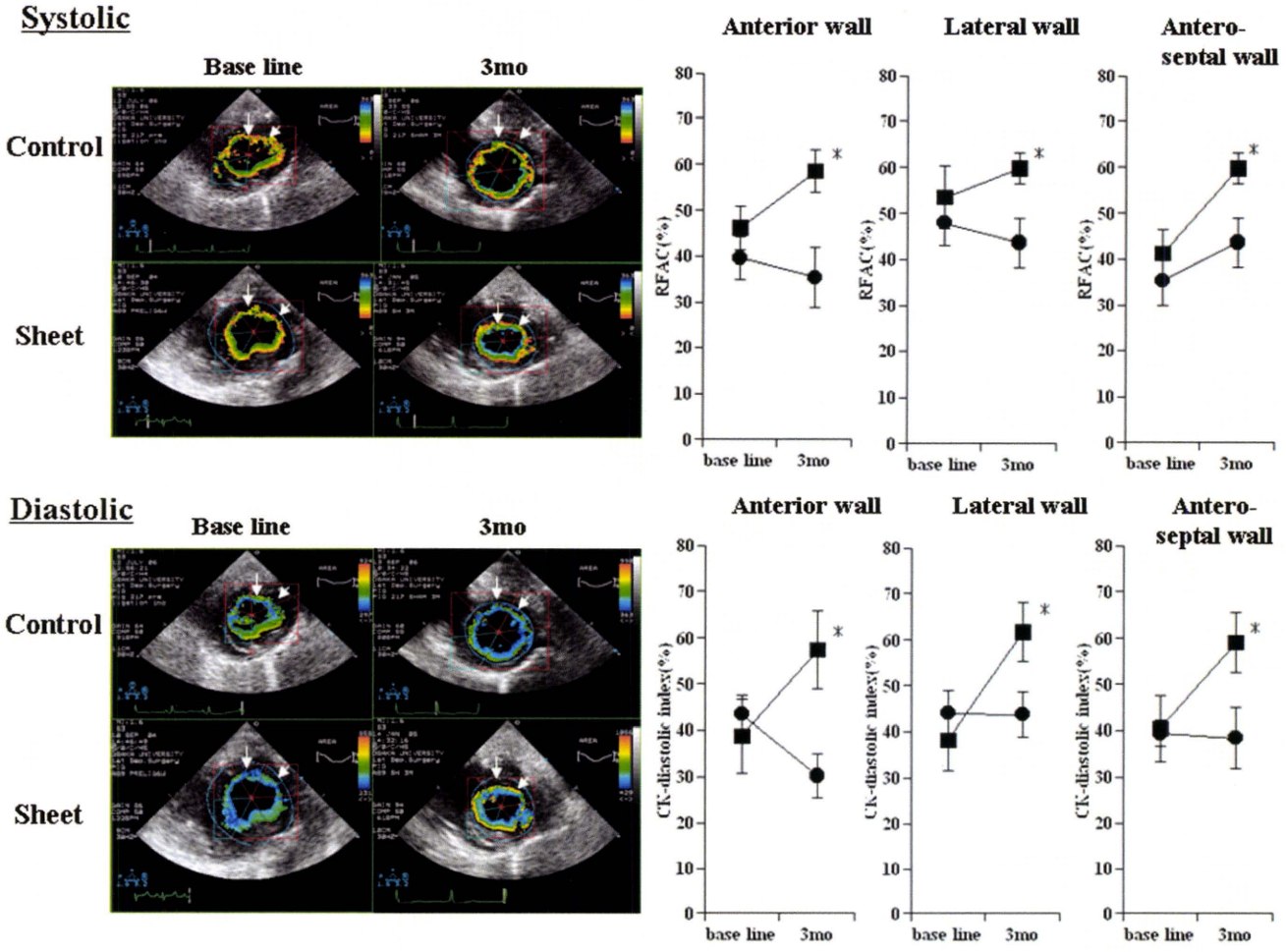

FIGURE 5. Systolic function: regional systolic function was significantly recovered in the skeletal cell (SC) group 3 months after implantation compared with the C group in the anterior, lateral, and anteroseptal wall. *P less than 0.05. Diastolic function: regional dysfunction was significantly recovered in the SC group 3 months after implantation compared with the C group in the anterior, lateral, and anteroseptal wall. Before treatment, diastolic dysfunction was observed in the infarction area of myocardium and the regional delayed relaxation was detected in the remote site of infarction by color kinesis. But this phenomenon was disappeared after SC sheet implantation. *P less than 0.05, ■: SC sheet, ●: control.

FAS (Fig. 4a) in the SC group compared with the C group (SC vs. C=49.5±2.8 vs. 24.6±2.0%, $P<0.05$). These functional improvements were preserved 6 months after implantation (SC vs. C=50.8±6.4 vs. 25.3±2.8%, $P<0.05$). The ESA was significantly smaller in the SC group than in the C group 3 months after the implantation (SC vs. C=4.3±0.5 vs. 9±1.3 cm^2, $P<0.05$) (Fig. 4b). These attenuation of LV dilatation were preserved 6 months after implantation (SC vs. C=4.9±0.8 vs. 7.5±1.4 cm^2, $P<0.05$). During this long-term observation, all SC sheet-treated animals were alive and exhibited no malignant arrhythmia assessed by 24-hour Holter ECG once a week (data not shown).

Before treatment, diastolic dysfunction was observed in the infarction area of myocardium and the regional delayed relaxation was detected in the remote site of infarction by color kinesis. After 3 months after implantation, CK-diastolic index in the lateral (SC vs. C=61.7±6.4 vs. 43.7±4.8%, $P<0.05$), anterior (SC vs. C=57.4±8.6 vs. 30.2±4.7%, $P<0.05$), and anteroseptal (SC vs. C=59±6.6 vs. 38.4±6.6%, $P<0.05$) segment were significantly ameliorated in the SC group compared with the C group, and regional systolic function in transplanted site was significantly improved in the SC group while not in the C groups (SC vs. C: lateral, 59.8±3.3 vs. 43.6±5.4%, $P<0.05$; anterior, 58.5±4.5 vs. 35.4±6.6%, $P<0.05$; anteroseptal, 59.8±3.3 vs. 43.6±5.4%, $P<0.05$), respectively (Fig. 5).

We could detect no ventricular premature beat for 24 hr by the Holter ECG in three myocardial infarction porcine received SC sheets.

Regional Myocardial Blood Flow and Residual Myocardial Tissue

PET study by using $^{15}0$-water showed that the myocardial water-perfusable tissue fraction and myocardial blood flow were higher in the anterior wall where SC sheets were implanted compared with the myocardium receiving no sheets. These data depict that myocardial blood flow was better and microcirculation in the infarcted myocardium was preserved in the SC sheets implanted myocardium. PET study by using ^{18}F-FDG revealed that more viable myocardial tis-

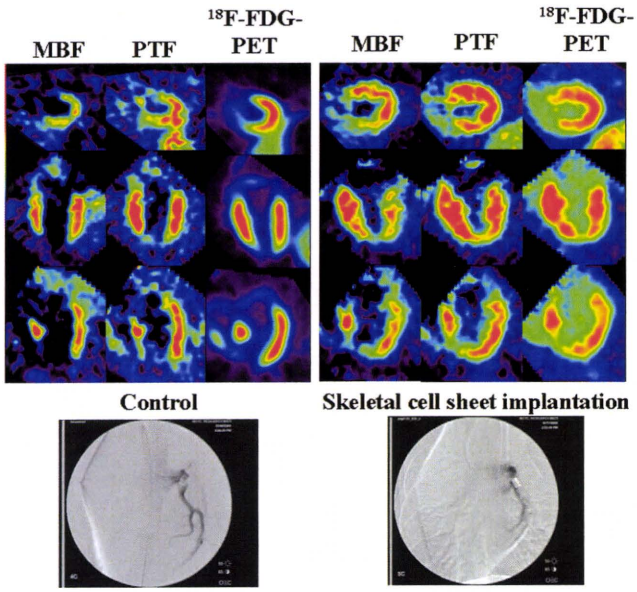

FIGURE 6. Positron emission tomography (PET) study revealed that perfusable tissue fraction (PTF) and myocardial blood flow (MBF) were higher and more viable myocardial tissues were preserved in the skeletal cell sheets implanted site compared with the myocardium receiving no sheets.

sues were preserved in the skeletal sheet implanted myocardium compared with the myocardium receiving no sheets. Coronary angiography revealed that LAD was occluded by the ameroid constrictor in both cases (Fig. 6).

DISCUSSION

Over the past several years, increasing awareness of the shortcomings of heart transplantation and left ventricular assist system implantation has led cardiovascular surgeons to consider alternative means of treating end-stage heart failure. In clinical setting, cellular cardiomyoplasty has been reported to have the potential of fundamental regenerative capability and has already been introduced in clinical trials with skeletal myoblast (*11*) or bone marrow mononuclear cells (*12*), and results suggest that it is a relatively feasible and safety therapy as a therapeutic angiogenesis. In this setting, cardiac tissue implantation was proposed to the treatment of end-staged heart failure as a new concept of regenerative therapy and experimentally some groups depicted it's effectiveness in the damaged myocardium (*13*, *14*). We also reported that cell sheets have great impacts on restoration of damaged myocardium in the rat infarction model (*3*, *4*) and dilated cardiomyopathy hamster (*5*). To convince the effectiveness of cell sheets in preclinical trial, we examined whether autologous SC sheets implantation might become one of the armamentarium of regenerative therapy for chronic heart failure caused by myocardial infarction in the porcine model.

The potential added advantages of the cell sheet implantation method include the implantation of a high number of cells with minimum cell loss. In contrast, the injection method is associated with a high loss of cells or surface proteins due to the trypsin treatment. Despite a high number of cell loss in needle injection, the cell sheet implantation method might provide the advantages of a higher number of cell implantation without cellular community destruction, leading the more improvement of cardiac performance rather than cell injection method (*4*). In case of needle injection, inflammation accompanied with destruction of myocardium induced by needle injection promotes graft death after cell transplantation (*15*).

To examine the effects of the SC sheet implantation therapy, we analyzed cardiac function and performed a histological assessment of the infarcted heart after SC sheet transplantation in a swine infarction model. SC sheet implantation therapy significantly induced angiogenesis, reduction of fibrosis histologically. And cell diameter of host myocyte was significantly attenuated its hypertrophy compared with the no treatment group. PET study revealed the better regional blood perfusion and better regional myocardial viability in the myocardium receiving cell sheets compared with the myocardium receiving no sheets.

Moreover, SC sheet implantation induced functional recovery of damaged myocardium. Especially, we demonstrated that the regional diastolic and systolic dysfunction was well recovered in the sheet implanted group. Before treatment, diastolic dysfunction of infarcted area and regional delayed relaxation of noninfarcted site were detected by color kinesis in the porcine infracted myocardium. After treatment, diastolic dysfunction of infarcted site was significantly recovered and the phenomenon of regional delayed relaxation in noninfarcted site was not seen. Presumably, implanted elastic myoblast sheets and a large quantity of well-developed smooth muscle cells, which are detected in the center of the scar, improved the regional diastolic dysfunction of implanted site. Although SC sheet can not contract in vivo after implantation, this recovery of diastolic disassociation of LV might result in the recovery of systolic dysfunction.

To the best of our knowledge, this is the first report in which tissue-engineered SC sheets implantation was successfully used to improve cardiac performance in a large animal model of ischemic myocardium according to the Laplace's theory.

The mechanisms of the restoration of damaged myocardium by SC sheet implantation might be complicated and many pathways might affect the recovery of ischemic myocardium. Recent reports depict that cell sheets enhance the recruitment of hematopoietic stem cells through the release of stromal-derived factor 1 (*4*). The fact of thicker anterior wall and the improvement of regional function might depend on both the recruitment of cytokine releasing stem cells, survival of grafted cells, and well-developed smooth muscle cells. And these cells might have good elasticity and these elastic cells and tissues softened the stiffness of anterior wall in association with the attenuating fibrosis even in the infarct area. This reduced stiffness of anterior wall might lead to the improvement of the diastolic dysfunction. Transplanted SCs cannot differentiate into cardiomyocyte anymore, but regional systolic function improved in the transplanted site. Probably, the improvement of regional diastolic function due to elastic cells might be responsible for the restoration of regional systolic dysfunction. Recent reports demonstrated that regional left ventricular myocardial relaxation was closely related to regional myocardial contraction (*16*) and the improvement of regional myocardial relaxation leads to the

recovery of global diastolic function (*17*). Moreover, the improvement of regional systolic function is closely related to global systolic function (*18*). We assume that this theory about the relationship between diastolic and systolic function is one of the mechanisms about the improvement of diastolic and systolic function in the cell sheet transplanted myocardium.

Question is why the well-developed smooth muscle cells exist in the center of the scar in the SC sheet group after transplantation despite a small quantity of smooth muscle cells in the SC sheet? Does a small quantity of smooth muscle cells in the SC sheet proliferate after transplantation? Do progenitor cells in the SC sheet differentiate to smooth muscle cells? Do progenitor cells or smooth muscle cells in the host myocardium migrate to the implanted site and proliferate? To the regret, there is no data to answer these questions exactly in this article and more detailed studies are needed to elucidate this important question.

Some reports depicted that the expression of hepatocyte growth factor (HGF) in the myoblast sheet transplanted ischemic myocardium is higher compared with the nontransplanted ischemic myocardium (*4*). HGF has an antifibrotic activity both through the activation of a matrix degradation pathway (*19*), restoration of cytoskeletal proteins on cardiomyocyte (*20*), and induce angiogenesis in the ischemic myocardium (*21*). Our study demonstrated that % fibrosis was significantly reduced in the SC sheet transplanted group. This paracrine secretion of HGF from SC sheets might attribute the reduction of % fibrosis. In our study, much more factor VIII-positive cells are detected in the SC sheet transplanted myocardium. This might be induced by paracrine secretion of HGF and angiogenesis might rescue the ischemic host cardiomyocyte and bring about the improvement of the distressed function of host cardiomyocyte. The distressed cytoskeletal proteins on the cardiomyocyte in the ischemic myocardium might be reorganized by the HGF secreted from skeletal sheet and the restoration of cytoskeletal proteins might lead to the improvement of cardiac function. And some reports demonstrated that myoblast sheets maintain the distressed cytoskeletal proteins on the host cardiomyocyte in the dilated cardiomyopathy hamster model (*5*). Consequently, cell sheet treatment is appropriate for recovery of ischemic cardiomyopathy. Recent research works demonstrated that several regenerative factors such as insulin-like growth factor-1 (*22*) and Thymosin b4 (*23*) were expressed in the rat ischemic myocardium model after myoblast sheet implantation by reverse-transcriptase polymerase chain reaction analysis (data not shown). After myoblast sheet transplantation to ischemic myocardium, several regenerative factors are expressed in the transplanted site, and these long-term and low-dosed expressed regenerative factors might cooperatively restore the damaged myocardium.

We could find no ventricular premature beat analyzed by Holter ECG after SC sheet implantation. We have already proved that in the rat infarction model, arrhythmia is less in the SC sheet implantation group compared with the needle injection group and this work represented that more monocyte chemotactic protein-1-positive cells and CD11b (macrophage marker)-positive cells were detected in the needle injection group compared with SC sheet implantation (data not shown). We speculate that needles destroy the myocardium and this destroyed myocardium may induce the inflammation and this inflammation may induce the arrhythmia. Conversely, SC sheet implantation technique normally doses not destroy the myocardium when they are implanted to recipient heart. Moreover, SC sheet will survive on the epicardium and electrical wave originated from implanted myoblasts may not deliver to the recipient myocardium directly. But when we implant myoblasts by needle injection, implanted myoblasts survive in the center of the myocardium and electrical wave will deliver to the myocardium directly, leading to the arrhythmia.

In conclusion, we have preclinically demonstrated SC sheets produced histologically and functionally apparent prevented the deterioration of the impaired myocardium in the swine model. These data provide a basis for attempting clinical cell sheet implantation in ischemic disease as the armamentarium to promote the regeneration of chronic heart failure caused by myocardial infarction.

ACKNOWLEDGMENTS

The authors thank Shigeru Matsumi and Masako Yokoyama for their excellent technical assistance.

REFERENCES

1. Shimizu T, Yamato M, Akutsu T, et al. Fabrication of pulsatile cardiac tissue grafts using a novel 3-dimensional cell sheet manipulation technique and temperature-responsive cell culture surfaces. *Circ Res* 2002; 90: e40.
2. Shimizu T, Sekine H, Isoi Y, et al. Long-term survival and growth of pulsatile myocardial tissue grafts engineered by the layering of cardiomyocyte sheets. *Tissue Eng* 2006; 12: 499.
3. Miyagawa S, Sawa Y, Sakakida S, et al. Tissue cardiomyoplasty using bioengineered contractile cardiomyocyte sheets to repair damaged myocardium: Their integration with recipient myocardium. *Transplantation* 2005; 80: 1586.
4. Memon IA, Sawa Y, Fukushima N, et al. Repair of impaired myocardium by means of implantation of engineered autologous myoblast sheets. *J Thorac Cardiovasc Surg* 2005; 130: 1333.
5. Kondoh H, Sawa Y, Miyagawa S, et al. Longer preservation of cardiac performance by sheet-shaped myoblast implantation in dilated cardiomyopathic hamsters. *Cardiovasc Res* 2006; 69: 466.
6. Hata H, Matsumiya G, Miyagawa S, et al. Grafted skeletal myoblast sheets attenuate myocardial remodeling in pacing-induced canine heart failure model. *J Thorac Cardiovasc Surg* 2006; 132: 918.
7. Mor-Avi V, Vignon P, Bales AC, et al. Acoustic quantification indexes of left ventricular size and function: Effects of signal averaging. *J Am Soc Echocardiogr* 1998; 11: 792.
8. Ishii K, Miwa K, Makita T, et al. Prolonged postischemic regional left ventricular delayed relaxation or diastolic asynchrony detected by color kinesis following coronary vasospasm. *Am J Cardiol* 2003; 91: 1366.
9. Fukui S, Kitagawa-Sakakida S, Kawamata S, et al. Therapeutic effect of midkine on cardiac remodeling in infarcted rat hearts. *Ann Thorac Surg* 2008; 85: 562.
10. Iida H, Yokoyama I, Agostini D, et al. Quantitative assessment of regional myocardial blood flow using oxygen-15-labelled water and positron emission tomography: A multicentre evaluation in Japan. *Eur J Nucl Med* 2000; 27: 192.
11. Dib N, Michler RE, Pagani FD, et al. Safety and feasibility of autologous myoblast transplantation in patients with ischemic cardiomyopathy: Four-year follow-up. *Circulation* 2005; 112: 1748.
12. Perin EC, Dohmann HF, Borojevic R, et al. Transendocardial, autologous bone marrow cell transplantation for severe, chronic ischemic heart failure. *Circulation* 2003; 107: 2294.
13. Leor J, Aboulafia-Etzion S, Dar A, et al. Bioengineered cardiac grafts. A new approach to repair the infarcted myocardium? *Circulation* 2000; 102(suppl III): III-56.

14. Li RK, Jia ZQ, Weisel RD, et al. Survival and function of bioengineered cardiac grafts. *Circulation* 1999; 100(suppl II): II-63.
15. Suzuki K, Murtuza B, Beauchamp JR, et al. Role of interleukin-1beta in acute inflammation and graft death after cell transplantation to the heart. *Circulation* 2004; 110(11 suppl 1): II-219.
16. Tanaka H, Kawai H, Tatsumi K, et al. Relationship between regional and global left ventricular systolic and diastolic function in patients with coronary artery disease assessed by strain rate imaging. *Circ J* 2007; 71: 517.
17. Tanaka H, Kawai H, Tatsumi K, et al. Improved regional myocardial diastolic function assessed by strain rate imaging in patients with coronary artery disease undergoing percutaneous coronary intervention. *J Am Soc Echocardiogr* 2006; 19: 756.
18. Moller JE, Hillis GS, Oh JK, et al. Wall motion score index and ejection fraction for risk stratification after acute myocardial infarction. *Am Heart J* 2006; 151: 419.
19. Liu Y, Rajur K, Tolbert E, et al. Endogenous hepatocyte growth factor ameliorates chronic renal injury by activating matrix degradation pathways. *Kidney Int* 2000; 58: 2028.
20. Miyagawa S, Sawa Y, Taketani S, et al. Myocardial regeneration therapy for heart failure: Hepatocyte growth factor enhances the effect of cellular cardiomyoplasty. *Circulation* 2002; 105: 2556.
21. Taniyama Y, Morishita R, Aoki M, et al. Therapeutic angiogenesis induced by human hepatocyte growth factor gene in rat and rabbit hindlimb ischemia models: Preclinical study for treatment of peripheral arterial disease. *Gene Ther* 2001; 8: 181.
22. Li Q, Li B, Wang X, et al. Overexpression of insulin-like growth factor-1 in mice protects from myocyte death after infarction, attenuating ventricular dilation, wall stress, and cardiac hypertrophy. *J Clin Invest* 1997; 100: 1991.
23. Bock-Marquette I, Saxena A, White MD, et al. Thymosin beta4 activates integrin-linked kinase and promotes cardiac cell migration, survival and cardiac repair. *Nature* 2004; 432: 466.

再生医療・細胞治療の規制に関する国際動向

Regulation of Cell Therapy Products and Tissue Engineered Products in EU and USA

佐藤 陽治　国立医薬品食品衛生研究所・遺伝子細胞医薬部・第2室　室長

〒158-8501 東京都世田谷区上用賀 1-18-1　Tel：03-3700-1141（代）　Fax：03-3707-6950
E-mail：yoji@nihs.go.jp

1　細胞・組織加工製品

治療法に乏しく，重篤・致死的ないしQOLを著しく損なう疾病・損傷に対する活路として，再生医療や細胞治療には非常に大きな期待が集まっている。これらの先進的な医療に用いることを目的として加工（培養・活性化・足場との複合化等）を施された細胞や組織，あるいは加工された細胞・組織を含む製品は「細胞・組織加工製品」（細胞・組織加工医薬品ないし細胞・組織加工医療機器）と呼ばれ，その開発は世界的にも熾烈な競争が展開している。ただし細胞・組織加工製品は，細胞という動的で複雑な成分を含むと同時に，その臨床応用に関して限られた経験と知識しか存在しないため，明確な科学的根拠に基づいた品質や安全性等の確保が課題となっており，比較的進んでいると言われる欧米においても，当局は実用化を促進するための試行を繰り返しながら規制の枠組みの整備を進めている。

2　規制の原則

欧米における細胞・組織加工製品の規制の原則は「リスクベースアプローチ」と呼ばれ，目的とする製品の性質に固有，かつその品質・安全性・有効性に関連するリスクの分析をベースにし，その影響の度合いを科学的に評価することにより規制や開発の方針・内容を定めるアプローチ方法が採られている。日本では，細胞・組織加工製品を医薬品・医療機器として開発するために薬事法に則って実施される「治験」と，細胞・組織加工製品を用いた治療法の開発を目的として医療法・医師法のもとで行われる「臨床研究」という異なる規制の枠組みが存在するが，欧米ではリスクベースアプローチの原則に基づき，商業目的か非商業目的かに拘わらず，原則的には同一の規制がかかる。即ち，大学病院等による非商業目的の「臨床研究」においても国への臨床試験申請並びにICH-GCP準拠が要求される点で日本よりも厳しい制度となっている。それでも開発が進む理由としては，研究資金・臨床試験支援体制などが充実している他，規制当局等の専門家が開発早期から開発者と情報を共有し，製品の目的に沿った柔軟な対応が可能となっていることなどが挙げられる。

3　EUの規制

欧州連合（EU）では細胞・組織加工製品は，製品中に含まれる細胞の作用様式に基づき体細胞治療薬（薬理学的･免疫学的又は代謝的機能）または組織工学製品（ヒト組織の再生・修復又は置換）に分類される。従来，体細胞治療薬は遺伝子治療薬とともにATMP（advanced therapy medicinal product）という医薬品の一類型に分類されていたが，2008年12月の制度改正により組織工学製品もATMPとして医薬品の規制を受けることになった。これと同時に，ATMPの販売承認については加盟国における審査を経ずに欧州医薬品庁（EMA）による中央審査によって行われるようになっており，制度改正からこれまでに培養軟骨製品1品目がATMPとして販売承認を受けている。なお制度改正以前に販売承認を

受けた製品については，新審査方式での販売承認を再取得しなければ，遺伝子治療薬・体細胞治療薬の場合には2011年末，組織工学製品の場合には2012年末に販売承認が取り消されることになっている。EMAはEUの医薬品産業の強化に必要な新技術の開発支援に積極的な姿勢を示しており，開発者に対するATMPに関する科学的助言や，中小開発企業の非臨床・品質データの暫定認証を行ったりすると同時に，研究開発が進むiPS細胞等の多能性幹細胞を加工したATMPに関する特別な留意点をまとめた文書を公表するなどしている。なお，EMAはあくまで販売承認審査を行う機関であり，臨床試験の開始・実施に関する手続きは加盟国の管轄となっている。加盟各国の規制当局もそれぞれ独自に，商業目的・非商業目的に拘わらず臨床試験開始前の開発早期から相談を安価ないし無料で受け付けるなど，ATMPの開発支援に積極的である。

4　米国の規制

米国ではヒト細胞・組織を利用した製品および遺伝子治療薬はHCT/P（human cell, tissue, or cellular/tissue-based product）と総称される。中でも細胞に一定以上の加工を施したものや遺伝子治療薬などは，州を越えて流通させる場合には公衆衛生サービス法351条により食品医薬品局（FDA）の販売承認が必要とされ，351HCT/Pと呼ばれる。EUとは異なり，351HCT/Pはその主な作用様式が細胞・組織の生化学的・免疫学的又は代謝的機能に基づく場合には生物製剤，細胞・組織の物理的又は構造的機能の場合には医療機器としての規制を受ける。これまでに2品目が生物製剤，5品目が医療機器として販売承認を受けている。EU同様，製品化を目的とするかどうかに関わらず，351HCT/Pの臨床試験を行う場合には，FDAに申請して承認を得る必要がある。近年の351HCT/Pの臨床試験申請の過半数は大学などによる非商業目的(研究目的)のものであるが，FDAは，生物製剤でも医療機器でも，商業目的・非商業目的に拘わらず臨床試験の申請前に非公式な相談を無料で行うほか，各種の開発段階において相談制度を設けて351HCT/Pの開発を支援している

5　おわりに

欧米の細胞・組織加工製品の開発に関する環境は，資金面，インフラ面の他，上に挙げたように規制に関しても日本とは大きく異なっている部分がある。ただし，細胞・組織加工製品を効率的・効果的・合理的に実用化するためには，必要な技術的要件や方策を，出口である行政側がガイドラインや相談制度などを通じて開発早期から提示し，研究者・開発企業・規制側が認識を共有することが不可欠であることは共通である。我が国における先端医療の実用化促進や規制の国際協調のためにも彼らの規制および促進策は参考とすべきものと考えられる。

THE JOURNAL OF BIOLOGICAL CHEMISTRY VOL. 285, NO. 20, pp. 15268–15277, May 14, 2010

Pertussis Toxin Up-regulates Angiotensin Type 1 Receptors through Toll-like Receptor 4-mediated Rac Activation*[S]

Received for publication, October 15, 2009, and in revised form, March 8, 2010 Published, JBC Papers in Press, March 15, 2010, DOI 10.1074/jbc.M109.076232

Motohiro Nishida[‡], Reiko Suda[‡], Yuichi Nagamatsu[‡], Shihori Tanabe[§], Naoya Onohara[‡], Michio Nakaya[‡], Yasunori Kanaho[¶], Takahiro Shibata[‖], Koji Uchida[‖], Hideki Sumimoto[**], Yoji Sato[§], and Hitoshi Kurose[‡1]

From the [‡]Department of Pharmacology and Toxicology, Graduate School of Pharmaceutical Sciences, and the [**]Department of Biochemistry, Graduate School of Medical Sciences, Kyushu University, Fukuoka 812-8582, the [§]Division of Cellular and Gene Therapy Products, National Institute of Health Sciences, Setagaya, Tokyo 158-8501, the [¶]Department of Physiological Chemistry, Graduate School of Comprehensive Sciences and Institute of Basic Medical Sciences, University of Tsukuba, Tsukuba 305-8575, and the [‖]Graduate School of Bioagricultural Sciences, Nagoya University, Nagoya 464-8601, Japan

Pertussis toxin (PTX) is recognized as a specific tool that uncouples receptors from G_i and G_o through ADP-ribosylation. During the study analyzing the effects of PTX on Ang II type 1 receptor (AT1R) function in cardiac fibroblasts, we found that PTX increases the number of AT1Rs and enhances AT1R-mediated response. Microarray analysis revealed that PTX increases the induction of interleukin (IL)-1β among cytokines. Inhibition of IL-1β suppressed the enhancement of AT1R-mediated response by PTX. PTX increased the expression of IL-1β and AT1R through NF-κB, and a small GTP-binding protein, Rac, mediated PTX-induced NF-κB activation through NADPH oxidase-dependent production of reactive oxygen species. PTX induced biphasic increases in Rac activity, and the Rac activation in a late but not an early phase was suppressed by IL-1β siRNA, suggesting that IL-1β-induced Rac activation contributes to the amplification of Rac-dependent signaling induced by PTX. Furthermore, inhibition of TLR4 (Toll-like receptor 4) abolished PTX-induced Rac activation and enhancement of AT1R function. However, ADP-ribosylation of G_i/G_o by PTX was not affected by inhibition of TLR4. Thus, PTX binds to two receptors; one is TLR4, which activates Rac, and another is the binding site that is required for ADP-ribosylation of G_i/G_o.

PTX,[2] a major virulence factor of Gram-negative bacillus *Bordetella pertussis*, which causes whooping cough, is well established as a pharmacological tool for a specific inhibitor of G_i signaling. PTX is composed of A-protomer and B-oligomer, and A-protomer exerts ADP-ribosyltransferase activity on the α subunit of heterotrimeric G_i proteins ($G\alpha_i$), leading to inhibition of receptor-G protein coupling (1, 2), whereas B-oligomer of PTX recognizes and binds carbohydrate-containing receptors that deliver A-protomer into the cytosol (3). However, several reports have demonstrated that PTX has additional effects, such as enhancement of immune responses (4–6), increase in adenosine A_1 receptor density (7), and activation of tyrosine kinase, mitogen-activated protein kinase, and NF-κB (8–10). These effects of PTX are reported to be independent of G_i modification.

Angiotensin (Ang) II plays an important role in the regulation of hypertrophy and/or hyperplasia of cardiovascular cells (11–13). In cardiac fibroblasts, Ang II has been demonstrated to stimulate the processes related to extracellular matrix remodeling (14). The biological function of Ang II is mediated by Ang II receptors located on the plasma membrane. Two isoforms (type 1 (AT1) and type 2 (AT2)) of Ang II receptor have been identified, but most of the cardiovascular effects of Ang II are attributed to AT1R (15). AT1R belongs to the G_q-coupled receptor family. Stimulation of AT1R activates phospholipase C and increases $[Ca^{2+}]_i$ through the production of inositol 1,4,5-trisphosphate, leading to the modulation of fibroblast activities, such as cell proliferation and extracellular matrix protein synthesis (16).

An increase in AT1R density is one of the features to enhance fibrogenic responses of the heart. For example, an increase in AT1R density has been reported in the heart after myocardial infarction (17, 18) and in hearts from biopsies from patients with spontaneous intracerebral hemorrhage (19). Several cytokines, such as tumor necrosis factor (TNF)-α and interleukin (IL)-1β, have been reported to up-regulate AT1R (17, 20). However, the molecular mechanism responsible for the increase in AT1R density is still unknown.

Many studies suggest that low concentration of ROS acts as a second messenger in the cardiovascular system (21, 22). Stimulation of IL-1β and TNF-α induces ROS production through

* This work was supported by grants from the Ministry of Education, Culture, Sports, Science, and Technology of Japan (to M. Nishida, M. Nakaya, and H. K.); a grant-in-aid for scientific research on Innovative Areas (to M. Nishida); a grant-in-aid for scientific research on Priority Areas (to H. K.); and grants from the Nakatomi Foundation, Sapporo Bioscience Foundation, and Naito Foundation (to M. Nishida).

[S] The on-line version of this article (available at http://www.jbc.org) contains supplemental Tables 1 and 2 and Figs. 1–4.

The data discussed in this study have been deposited in the NCBI Gene Expression Omnibus (GEO) (http://www.ncbi.nlm.nih.gov/geo) and are accessible through GEO Series accession number GSE5017.

[1] To whom correspondence should be addressed. Tel./Fax: 81-92-642-6884; E-mail: kurose@phar.kyushu-u.ac.jp.

[2] The abbreviations used are: PTX, pertussis toxin; Ang II, angiotensin II; AT1R, Ang II type 1 receptor; DN-Rac and DN-$p47^{phox}$, dominant negative Rac and $p47^{phox}$, respectively; DPI, diphenyleneiodonium; GFP, green fluorescent protein; ct, carboxyl terminal region; IκBαm, non-phosphorylated form of IκBα, which works as a dominant negative mutant; IL, interleukin; MOI, multiplicity of infection; NF-κB, nuclear factor κB; IκB, inhibitor of κB; PH, pleckstrin homology; PI, phosphatidylinositol; PI-3-P, PI 3-phosphate; PLC, phospholipase C; PX, *phox* homology; Ro-106-9920, 6-(phenylsulfinyl)tetrazolo[1,5-*b*]pyridazine; ROS, reactive oxygen species; TNF-α, tumor necrosis factor-α; WT, wild type; ELISA, enzyme-linked immunosorbent assay; siRNA, small interfering RNA.

NADPH oxidase activation (23). A small GTP-binding protein, Rac, regulates the activity of NADPH oxidase (24) and mediates IL-1β- or TNF-α-induced ROS production and NF-κB activation (25). We have previously reported that Rac mediates Ang II-stimulated ROS production through NADPH oxidase activation in cardiac myocytes and cardiac fibroblasts (26, 27). Overexpression of constitutively active Rac1 induces hypertrophic responses in isolated cardiomyocyte and dilated cardiomyopathy *in vivo* (28, 29). Although a high concentration of hydrogen peroxide (H_2O_2) is reported to decrease AT1R density (30), it is unknown whether production of low concentration of ROS via Rac-mediated NADPH oxidase activation participates in the receptor-stimulated increase in AT1R density of cardiac cells.

Toll-like receptors (TLRs) play a critical role in both innate and adaptive immunity (31). There are at least 10 TLRs identified so far in humans, which specifically recognize and bind to a variety of pathogenic factors, including lipopolysaccharide. The mouse heart expresses at least six receptors (TLR2, -3, -4, -5, -7, and -9), and the stimulation of these receptors induces activation of NF-κB. TLR2 and TLR4 have been extensively studied in the heart, and both receptors are in part responsible for cardiac dysfunction in certain pathological conditions (32). Recent studies have elucidated that PTX functions as a superior ligand for TLR4 (6, 10). Although stimulation of TLR4 results in production of proinflammatory cytokines, it has not been reported that PTX exerts some pharmacological action(s) through TLR4 in cardiovascular cells, and it is unknown whether PTX-induced ADP-ribosylation of G_i/G_o requires TLR4-mediated entry into cells.

During the study of the role of G_i proteins in AT1R-mediated fibrotic responses using rat neonatal cardiac fibroblasts, we found that PTX enhances Ang II-induced increase in $[Ca^{2+}]_i$. Because we previously reported that the treatment with PTX increases Rac activity in rat neonatal cardiac myocytes (26), we hypothesized that Rac is implicated in PTX-induced enhancement of Ang II signaling in cardiac fibroblasts. In this study, we demonstrate that PTX B-oligomer induces Rac activation through a pathway independent of ADP-ribosylation of G_i/G_o. PTX increases IL-1β induction through sequential activation of TLR4, Rac, NADPH oxidase, and NF-κB, which leads to AT1R up-regulation through amplification of Rac-dependent signaling in rat cardiac fibroblasts.

EXPERIMENTAL PROCEDURES

Materials, Recombinant Adenoviruses, and Culture of Cardiac Fibroblasts—PTX, simvastatin, and anti-$G\alpha_{q/11}$ antibody were purchased from Calbiochem. Ang II was from Peptide Institute. Mastparan-7, ATP, wortmannin, and diphenyleneiodonium (DPI) were purchased from Sigma. Ro-106-9920 was from Tocris. Rat IL-1β and PTX B-oligomer were from Wako. Rabbit anti-rat IL-1β antibody and the rat IL-1β ELISA kit were from Endogen. Anti-$G\alpha_{11}$, anti-PLCβ_3, anti-IκBα, anti-p65, anti-RhoA, anti-rabbit IgG, and anti-mouse IgG antibodies were purchased from Santa Cruz Biotechnology, Inc. (Santa Cruz, CA). [^{125}I]Ang II, [^{32}P]NAD, and glutathione-Sepharose beads were from Amersham Biosciences. Anti-Rac1 and anti-Rap1 antibodies were from Transduction Laboratories. Anti-Ras antibody was from Upstate Biotechnology. Anti-phospho-Akt and anti-Akt antibodies were from Cell Signaling. Fura2/AM was from Dojindo. 2,7-dichlorofluorescein diacetate and Alexa Fluor 488 goat anti-rabbit antibody were from Molecular Probes. Collagenase and Fugene 6 were from Roche Applied Science. Dual luciferase reagents were from Promega. pNF-κB-Luc and pRL-SV40 were from Stratagene. The sequences coding the Rap1-binding domain of Ral-GDS, Rac-binding domain of p21-activated kinase, Rho-binding domain of rhotekin, or Ras-binding domain of Raf were cloned, sequenced, and ligated into pGEX-4T-1 to make glutathione *S*-transferase fusion protein constructs. Glutathione *S*-transferase fusion proteins were expressed at room temperature and purified using gluthathione-Sepharose as described (33). The cDNA encoding GRP1-PH was provided by Dr. Alexander Gray (University of Dundee, Scotland). Recombinant adenoviruses of GRK2 (G protein-coupled receptor kinase 2)-ct, RGS4 (regulator of G protein signaling 4), WT $G\alpha_i$, $G\alpha_i$-ct, IκBαm, GFP-fused WT Rac, GFP-fused constitutively active Rac (G12V), DN-Rac (T17N), DN-p47^{phox}, and p115-RGS were produced as described previously (26, 34). Stealth siRNAs oligonucleotides for rat IL-1β, TLR4, and Rac1 were from Invitrogen. Sequences of stealth siRNA used were described in supplemental Table 1. Cardiac fibroblasts were prepared from ventricles of 1–2-day-old Sprague-Dawley rats, as described previously (27).

Quantification of Intracellular Ca^{2+} and ROS Concentration—$[Ca^{2+}]^i$ was measured by the method described previously (35). Briefly, cells (5×10^4) were plated on a 3 × 10-mm microcoverglass (MATSUNAMI) and loaded with 1 μM fura-2/AM in the cultured medium at 37 °C for 30 min. Cells were washed with HEPES-buffered salt solution containing 107 mM NaCl, 6 mM KCl, 1.2 mM $MgSO_4$, 0.5 mM EGTA, 20 mM HEPES (pH 7.4), and 11.5 mM glucose. Measurement of intracellular ROS concentration was performed in 2 mM Ca^{2+}-containing HEPES-buffered salt solution with a fluorescent dye, 2,7-dichlorofluorescein diacetate, as described previously (27). Fluorescence images were recorded and analyzed with a video image analysis system (Aquacosmos, Hamamatsu Photonics). The peak changes ($\Delta F/F_0$) of dichlorofluorescein fluorescence intensity were identified as values obtained by subtracting the basal fluorescence intensity (F_0) from the maximal intensity during a 15-min PTX treatment.

Measurement of IL-1β mRNA and Protein Expression—Expression of IL-1β mRNA and protein was measured by real time reverse transcription-PCR and ELISA, as described previously (36). For the preparation of real time reverse transcription-PCR analysis, cells (3×10^5) plated on 6-well dishes were treated with PTX for 24 h and lysed with 400 μl of RLT buffer (Qiagen). For ELISA, cells (1×10^5) on 12-well dishes were treated with PTX (100 ng/ml) in 500 μl of medium, and cells were then collected together with medium. After cells were homogenized with a 26-gauge syringe, 100 μl of supernatants were used. Assays were performed according to the manufacturer's instructions.

Microarray Analysis—Cells (1×10^6) plated on 35-mm dishes were treated with PTX for 24 h and lysed with 400 μl of RLT buffer. Total RNA was extracted with the RNeasy minikit (Qiagen) and RNase-free DNase set (Qiagen). Total RNA was converted to biotin-labeled cRNA, which was hybridized to the

rat genome U34A GeneChip (Affymetrix) for 16–24 h at 45 °C. The hybridization signals on the microarray were scanned and computed at a target intensity of 500 by a GeneChip Scanner 3000 and GeneChip Operating Software (Affymetrix), respectively. The data analysis was performed as follows. At the first step, probe sets without expression in the fibroblasts, which were indicated as absent by absolute analysis in more than half of the replicates in both the control and PTX-treated groups, were eliminated from the data set. Then, if the difference in the mean signal intensity of a given probe set was equal to the cut-off (1.25-fold) or more between the control and PTX-treated groups and if its p value calculated by Student's t test was less than 0.05, that probe set was employed. At the last step, probe sets with an annotation "signal transduction" (GO:0007165) in the AmiGO data base (available on the World Wide Web) were extracted, using the NetAffx Gene Ontology Mining Tool (available on the World Wide Web).

Ang II Binding Assay—Measurement of Ang receptor binding was performed according to the previous report (15) with a slight modification. After various treatments for 24 h, cardiac fibroblasts were rinsed with 10 ml of ice-cold phosphate-buffered saline and mechanically detached in 1 ml of ice-cold lysis buffer containing 10 mM Tris, pH 7.4, 5 mM EDTA, 5 mM EGTA, 1 μg/ml benzamidine, 10 μg/ml soybean trypsin inhibitor (type II-S), and 5 μg/ml leupeptin. The cell lysate was centrifuged at 45,000 × *g* for 10 min at 4 °C. The pellet containing crude membrane fraction was resuspended in 1 ml of ice-cold lysis buffer with a Potter type homogenizer, frozen, and stored at −80 °C until use. After the concentration of membrane protein was determined, membrane protein (20 μg) was used for the binding studies. The membrane was incubated with 0.1 nM ^{125}I-Ang II in 75 mM Tris, pH 7.4, 12.5 mM $MgCl_2$, 2 mM EDTA, and increasing concentrations of unlabeled Ang II (0–14 nM) for 1 h at 25 °C. Nonspecific binding was determined in the presence of 1 μM unlabeled Ang II. The reaction mixture was filtered over Whatman GF/C filters. The filters were washed with ice-cold buffer containing 25 mM Tris, pH 7.4, and 1 mM $MgCl_2$. The bound ^{125}I-Ang II on the filters was measured with a γ-counter. The values of K_d and B_{max} were calculated by Prism software (GraphPad Software, San Diego, CA).

Measurement of NF-κB Activity—After adenovirus was infected at 100 MOI for 2 h in serum-free medium, fibroblasts (3×10^5 cells) in a 24-well plate were transiently co-transfected with 0.45 μg of pNF-κB-Luc and 0.05 μg of pRL-SV40 control plasmid, using Fugene 6 (27). Luciferase activity was measured 48 h after transfection with dual luciferase reagents.

Measurement of Small GTPase Activities—Activation of small G proteins was determined as described previously (26). Activated Rac, Rho, Ras, and Rap1 were pulled down with 5 μg of glutathione *S*-transferase-fused Rac-interacting domain of p21-activated kinase (PAK-CRIB), Rho-binding domain of rhotekin (34), Ras-binding domain of Raf-1 (37), and Rap1-binding domain of Ral-GDS (38), respectively. Pulled-down small G proteins were detected with anti-Rac1, anti-RhoA, anti-Ras and anti-Rap1 antibodies. For knockdown of Rac1, cells were transfected with a mixture of Rac1 siRNAs (50 nM each) for 72 h.

Confocal Visualization of GFP-fused Proteins and NF-κB p65 Subunit—Cells (1×10^5) plated on glass bottom 35-mm dishes were infected for 24 h with GFP, GFP-Rac, GFP-constitutively active Rac, GFP fusion protein with PX domain of $p40^{phox}$ ($p40^{phox}$-PX), and $p40^{phox}$-PX (R105K). After the treatment with PTX (100 ng/ml) for 24 h, cells were fixed by 10% formaldehyde neutral buffer solution. For localization of NF-κB, cells were stained with anti-p65 antibody. Fluorescence images were measured at an excitation wavelength of 488 nm with a laser-scanning confocal imaging system (Carl Zeiss LSM510).

In Vitro PTX-catalyzed ADP-ribosylation Assay—*In vitro* ADP-ribosylation of $G\alpha_i$ proteins by PTX was performed as described previously (39) with a slight modification. Briefly, cardiac fibroblasts pretreated with or without 100 ng/ml PTX for 24 h were harvested with ice-cold lysis buffer containing 50 mM Tris (pH 7.5), 5 mM EDTA, 5 mM EGTA, 10 μg/ml benzamidine, 5 μg/ml aprotinin, and 5 μg/ml leupeptin. After centrifugation at 15,000 rpm for 10 min at 4 °C, the pellet was resuspended in lysis buffer. PTX was preactivated by incubation in the solution containing 50 mM Tris (pH 7.5), 5 mM ATP, 20 mM dithiothreitol, and 1 mg/ml bovine serum albumin for 30 min at 30 °C. Then activated PTX was added to the assay mixture, including 100 μg of the membrane, and incubated for 60 min at 30 °C. The final concentrations of all reagents in the assay mixture were as follows: 50 mM Tris (pH 7.5), 50 μM GDP, 10 mM thymidine, 5 μM NAD, 0.5 μM [^{32}P]NAD, 20 μg/ml PTX, 0.2 mg/ml bovine serum albumin, 1 mM ATP, and 4 mM dithiothreitol. The reaction was stopped by the addition of an excessive amount of ice-cold 50 mM Tris (pH 7.5), and the samples were centrifuged at 15,000 rpm for 10 min at 4 °C. The pellet was solubilized in SDS sample buffer, boiled, and subjected to 12% SDS-PAGE. Radioactive bands were detected by filmless autoradiographic analysis (BAS2000 system, Fujifilm).

Statistical Analysis—The results are presented as mean ± S.E. from at least three independent experiments. The representative data of time course experiments were plotted from one of three similar experiments that were performed with more than 20 cells. The mean values were compared with control by one-way analysis followed by Dunnet's t test (for three or more groups) or Student's t test (for two groups).

RESULTS

PTX Enhances Ang II-induced Ca^{2+} Release through AT1R Up-regulation—During the study of AT1R function in cardiac fibroblasts, we found that treatment with PTX enhances transient increase in $[Ca^{2+}]_i$ induced by Ang II at low concentration in the absence of extracellular Ca^{2+} (Fig. 1*A*). The EC_{50} value of Ang II for the changes in $[Ca^{2+}]_i$ increases was 464 ± 44 pM in control cells, whereas the EC_{50} value was decreased to 91 ± 33 pM in PTX-pretreated cells (Fig. 1*B*). However, the ATP-induced Ca^{2+} release was not affected by PTX (Fig. 1*C*). These results suggest that PTX selectively enhances Ca^{2+} response induced by AT1R stimulation. We also found that treatment with PTX for 24 h resulted in a 2-fold increase in maximal ^{125}I-Ang II binding activity (B_{max}) in comparison with PTX-untreated membrane (Fig. 1*D*). PTX increased AT1R density in a time-dependent manner, and more than 18 h was required for a 2-fold increase in AT1R density (supplemental Fig. 1). The

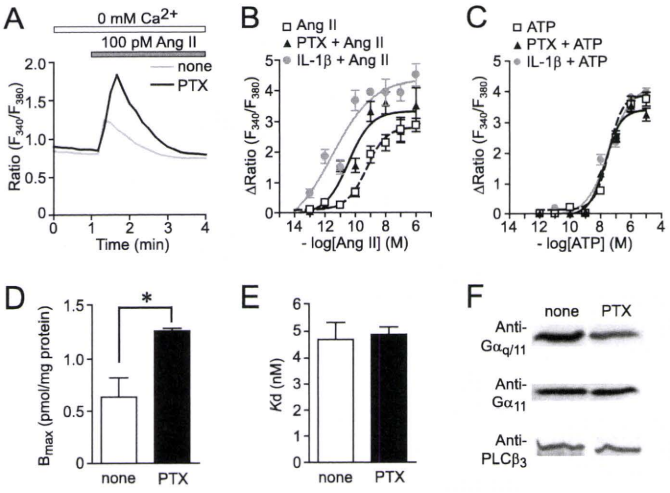

FIGURE 1. **PTX enhances Ca^{2+} responses by Ang II through AT1R up-regulation.** *A*, average time courses of Ca^{2+} response induced by Ang receptor stimulation with Ang II (100 pM) in control and PTX-treated cells. *B* and *C*, peak increases in $[Ca^{2+}]_i$ ($\Delta Ratio$) plotted against various concentrations of Ang II (*B*) and ATP (*C*) in control, PTX-treated, and IL-1β-treated cells. Cells were treated with PTX (100 ng/ml) or IL-1β (10 ng/ml) for 24 h before agonist stimulation. *D* and *E*, increases in AT1R density induced by PTX (100 ng/ml) for 24 h. The B_{max} (*D*) and K_d (*E*) values for Ang II binding were calculated with GraphPad Prism software. *F*, effects of PTX on expression of $G\alpha_{q/11}$ and $PLC\beta_3$. *, $p < 0.05$ *versus* PTX-untreated cells. *Error bars*, S.E.

PTX-induced increase in B_{max} was completely suppressed by CV11974 (1 μM, AT1R-selective blocker) but not by PD123319 (1 μM, AT2R-selective blocker) (data not shown). The K_d value was not affected by PTX (Fig. 1*E*), indicating that the PTX-induced enhancement of AT1R function is not explained by structural changes in AT1R. It has been reported that the increased expression of $G\alpha_{q/11}$ and $PLC\beta_3$ is involved in the enhancement of Ang II-induced Ca^{2+} responses in the ischemic heart (40, 41). However, PTX did not affect the expression levels of $G\alpha_q$, $G\alpha_{11}$, and $PLC\beta_3$ (Fig. 1*F*). These results suggest that the enhancement of Ang II-induced Ca^{2+} release in PTX-treated cells is due to AT1R up-regulation but not up-regulation of components of the $G\alpha_q$-$PLC\beta$ pathway.

Because commercially available PTX contaminates with other endotoxins, including lipopolysaccharide, it is possible that other endotoxins contribute to enhancement of AT1R function. Thus, we examined the effects of denatured PTX or PTX purchased from another manufacturer (Sigma) on AT1R functions. Pretreatment of PTX with heat significantly reduced the enhancement of Ang II-induced Ca^{2+} release induced by PTX (supplemental Fig. 1). In contrast, the Ang II-induced Ca^{2+} release was also enhanced by PTX purchased from Sigma as well as that induced by PTX from Calbiochem. These results suggest that PTX proteins *per se* induce AT1R up-regulation in cardiac fibroblasts.

IL-1β Production Induced by PTX Treatment—To examine whether PTX treatment induces production of a factor(s) that participates in up-regulation of AT1R, we performed microarray analysis of mRNAs from PTX-treated fibroblasts. For each gene, we calculated the average intensity in expression for both control and PTX-treated cells and plotted the ratio of these two induction values. Genes were chosen whose expression was at least 1.25-fold increased or decreased as compared with control cells. The probe sets of 405 genes showed significant changes by PTX treatment. Genes were then assigned to several groups according to their function, and we picked out 70 genes in the gene cluster that is termed "signal transduction" in the AmiGO data base (supplemental Table 2). PTX treatment selectively increased AT1R mRNA (Fig. 2*A*) but not other G protein-coupled receptors. Among genes increased by PTX treatment, IL-1α and IL-1β mRNAs showed a marked increase in expression (Fig. 2*A*). Real-time PCR confirmed the strong induction of IL-1β mRNA by PTX treatment (Fig. 2*B*). Although PTX is reported to increase IL-12 expression by inhibition of G_i signaling in T lymphocytes (42), PTX did not significantly increase mRNA expression of other cytokines (supplemental Table 1). Treatment with mastoparan-7 or the expression of WT $G\alpha_i$ or inhibitory polypeptides of G_i signaling ($G\alpha_i$-ct, a polypeptide that specifically inhibits receptor-G_i protein coupling (39); RGS4, a GTPase-activating protein that specifically binds the GTP-bound form of $G\alpha_i$ and $G\alpha_q$ (43); and GRK2-ct, a $G\beta\gamma$ ($\beta\gamma$ subunit of heterotrimeric G protein)-sequestering polypeptide (44)) did not increase IL-1β mRNA expression (Fig. 2*B*). We also confirmed that the expression of $G\alpha_i$-ct did not enhance Ang II-induced Ca^{2+} release (data not shown), and the treatment with B-oligomer of PTX enhanced Ang II-induced Ca^{2+} release (Fig. 2*C*). Furthermore, ELISA revealed that the treatment with PTX actually increased the expression of IL-1β protein levels, whereas the expression of IL-1α protein was below the detection level in PTX-treated cardiac fibroblasts (Fig. 2*D*). These results suggest that PTX selectively induces IL-1β production, and G_i modification is not required for PTX-induced IL-1β production.

IL-1β Mediates PTX-induced Enhancement of Ang II-induced Ca^{2+} Response—Because it has been reported that IL-1β increases AT1R density in cardiac fibroblasts (17, 45), the cells were treated with IL-1β. Treatment with IL-1β (10 ng/ml) enhanced Ang II-induced Ca^{2+} release ($EC_{50} = 31 \pm 26$ pM) but not ATP-induced Ca^{2+} release, in rat cardiac fibroblasts (Fig. 1, *B* and *C*). These effects of IL-1β are similar to the effects of PTX treatment, and the enhancement by IL-1β seems to be consistent with the findings that PTX treatment increased the induction of IL-1β mRNA and protein. Thus, we examined whether PTX-induced IL-1β production participates in the enhancement of AT1R function. The PTX-induced IL-1β production was suppressed by the treatment with IL-1β siRNAs (Fig. 2*E*). The enhancement of Ang II-induced Ca^{2+} release by IL-1β treatment was almost completely suppressed by anti-IL-1β neutral antibody (Fig. 2*F*), indicating that the antibody sufficiently inhibits IL-1β-mediated responses. The enhancement of Ang II-induced Ca^{2+} release by PTX was also suppressed by anti-IL-1β antibody and IL-1β siRNAs (Fig. 2*G*), indicating that PTX-induced IL-1β secretion mediates the enhancement of Ang II-induced Ca^{2+} release.

Involvement of NF-κB in PTX-induced IL-1β Expression—As the promoter regions of IL-1β and AT1R contain a putative NF-κB binding site (46–48), we next examined the involvement of NF-κB in PTX-induced IL-1β production. As shown in Fig. 3*A*, PTX-induced increase in IL-1β mRNA expression was suppressed by the treatment with Ro-106-9920, a selective inhibitor of IκB phosphorylation, and by the expression of a dominant negative IκB, IκBαm. Because Ro-106-9920 showed

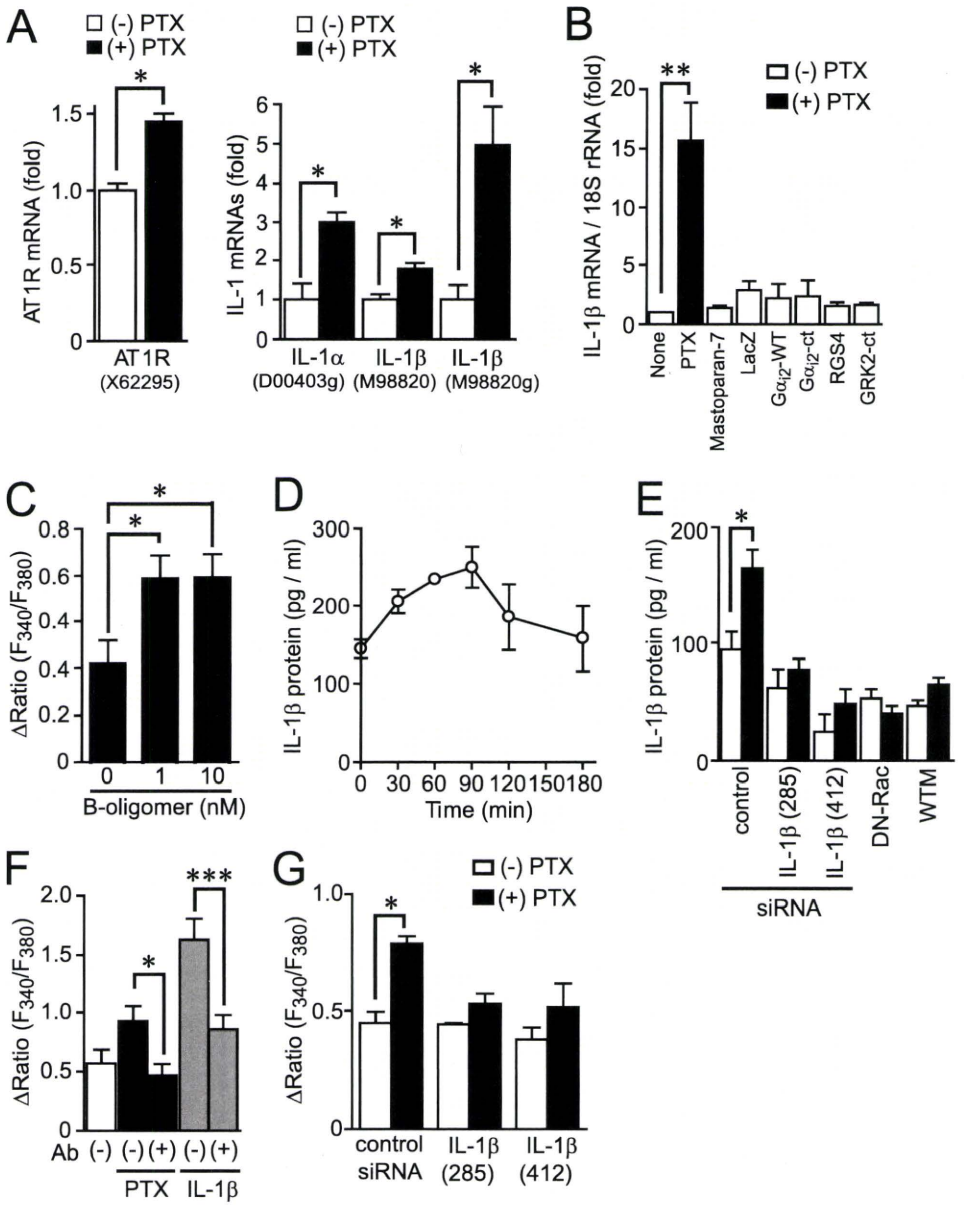

FIGURE 2. **Involvement of IL-1β production in PTX-induced enhancement of Ca^{2+} response by Ang II stimulation.** *A*, effects of PTX on the expression of AT1R, IL-1α, and IL-1β mRNAs. After cells were treated with PTX (100 ng/ml) for 24 h, total RNA was extracted. The expression of mRNAs was determined with microarray analysis. ID numbers of primer probe sets are shown in *parenthesis*. *B*, effects of respective reagents on IL-1β mRNA expression in cardiac fibroblasts. Cells were treated with PTX (100 ng/ml) for 24 h, treated with mastoparan-7 (10 μM) for 12 h, or infected with LacZ, WT $G\alpha_i$, $G\alpha_i$-ct, RGS4, and GRK2-ct at 300 MOI for 48 h. The -fold increases were calculated by the values of untreated cells (none) set as 1. *C*, effects of B-oligomer of PTX on Ang II-induced Ca^{2+} releases. Cells were treated with B-oligomer (1 or 10 nM) for 24 h before Ca^{2+} measurement. *D*, time course of PTX-induced expression of IL-1β protein. *E*, effects of IL-1β siRNAs, DN-Rac, and wortmannin (*WTM*) on PTX-induced IL-1β production. Two different siRNAs were used. *F* and *G*, effects of IL-1β neutral antibody (*F*) or IL-1β siRNAs (*G*) on Ang II-induced Ca^{2+} responses in control, PTX-treated, or IL-1β-treated cells. Cells were treated with PTX (100 ng/ml) or IL-1β (1 ng/ml) for 24 h before Ang II (100 pM) stimulation with or without anti-IL-1β antibody (500 μg/ml). Cells were transfected with IL-1β siRNAs (100 nM) 48 h before PTX treatment. *, $p < 0.05$; **, $p < 0.01$; ***, $p < 0.001$ *versus* PTX-untreated, B-oligomer-untreated, control siRNA-treated, PTX-treated, or IL-1β-treated cells. *Error bars*, S.E.

cytotoxic effects at higher concentration, we could not increase the concentration to observe complete inhibition of the IL-1β induction. The enhancement of AT1R function by PTX was suppressed by Ro-106-9920 and IκBαm (Fig. 3*B*), and the PTX-induced increase in AT1R density was suppressed by IκBαm (Fig. 3, *C* and *D*). Because an inhibition of NADPH oxidase activity suppresses NF-κB activation and IL-1β production induced by $G\alpha_{13}$ activation (36), we next examined the involvement of NADPH oxidase. Treatment with PTX increased NF-κB-dependent luciferase activity (Fig. 3, *E* and *F*). This NF-κB activation was suppressed by the treatment with DPI or by the expression of dominant negative (DN)-Rac and DN-$p47^{phox}$, both of which are essential for NADPH oxidase activation (24), but not by p115-RGS, a $G\alpha_{13}$-inhibitory polypeptide (26). These results suggest that PTX induces NF-κB activation through Rac-NADPH oxidase pathway and that NF-κB mediates PTX-induced IL-1β production and AT1R up-regulation.

Rac Mediates PTX-induced IL-1β Production and AT1R Up-regulation—We have previously reported in rat neonatal cardiomyocytes that PTX increases basal Rac activity (26). Because the PTX-induced NF-κB activation and IL-1β production was suppressed by DN-Rac (Figs. 2 and 3), we next examined whether PTX increases Rac activity in cardiac fibroblasts. Rac was activated from 10 min after PTX treatment and still activated at 24 h after the treatment (Fig. 4*A*). We also found that PTX did not affect the activities of other small G proteins, Ras, Rap1, and RhoA (supplemental Fig. 2). It has been reported that phosphatidylinositol (PI) 3-kinase participates in PTX B-oligomer-induced antiapoptotic action against HIV-Tat infection in NK cells (49). We confirmed that PTX B-oligomer increased Rac activity in cardiac fibroblasts (supplemental Fig. 3). Pretreatment with wortmannin completely suppressed PTX-induced Rac activation (Fig. 4*B*). The activated Rac has been reported to translocate from cytosol to the plasma membrane through recognition of membrane phospholipids, such as PI 3-phosphate (PI-3-P), PI 4-phosphate, PI 5-phosphate, and PI 3,4,5-trisphosphate, through the carboxyl-terminal polybasic region of Rac (50–52). Confocal imaging revealed that PTX actually translocated GFP-fused WT Rac from cytosol to the plasma membrane, as observed with constitutively active Rac (Fig. 4*C*). Pretreatment with wortmannin inhibited PTX-induced membrane localization of Rac. To demonstrate the involvement of PI-3-P, $p40^{phox}$-

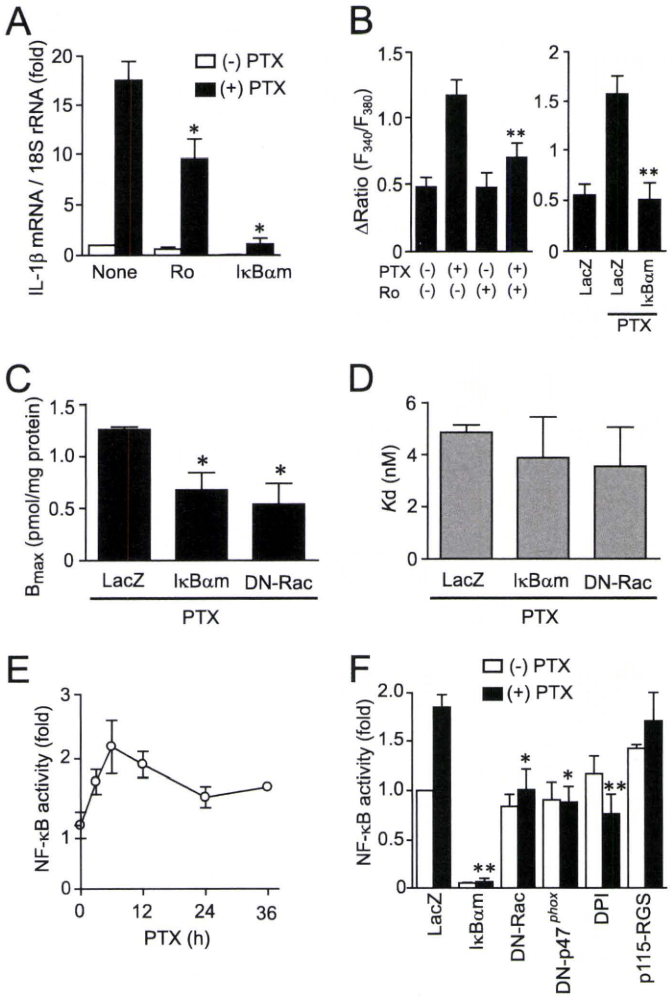

FIGURE 3. **Requirement of NF-κB for PTX-induced enhancement of Ca^{2+} response by Ang II stimulation.** *A*, effects of Ro106-9920 and IκBαm on PTX-induced IL-1β mRNA expression. Cells were pretreated for 20 min with Ro106-9920 (1 μM) or infected with IκBαm (100 MOI) for 48 h before the treatment of PTX (100 ng/ml) for 24 h. *B*, effects of NF-κB inhibitors on Ang II-induced Ca^{2+} responses in PTX-treated cells. *C* and *D*, effects of IkBαm and DN-Rac on PTX-induced increase in AT1R density. Cells were infected with adenoviruses expressing IkBαm or DN-Rac 24 h before PTX treatment. AT1R density was determined with receptor binding assay. *E*, time course of PTX-induced changes in NF-κB-dependent luciferase activity. *F*, effects of IκBαm, DN-Rac, DN-p47^{phox}, DPI, and p115-RGS on PTX-induced NF-κB activation. Cells were infected with LacZ, IκBαm, DN-Rac, DN-p47^{phox}, or p115-RGS at 100 MOI for 48 h or pretreated with DPI (5 μM) for 20 min before the addition of PTX (100 ng/ml) for 6 h. *, $p < 0.05$; **, $p < 0.01$ *versus* PTX-untreated or LacZ-expressing cells. *Error bars*, S.E.

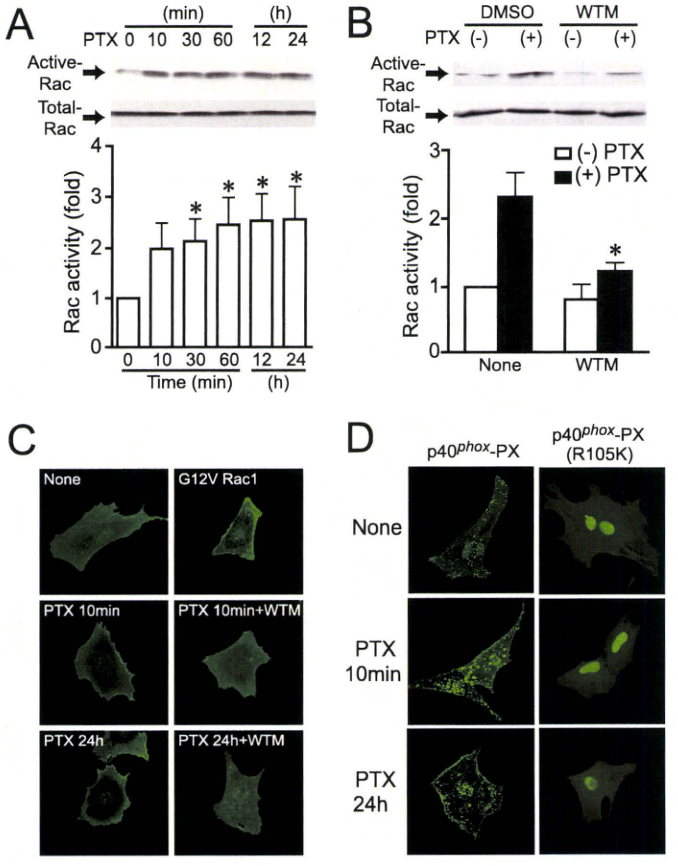

FIGURE 4. **PTX induces Rac activation.** *A*, time course of Rac activation induced by PTX (100 ng/ml). *B*, effects of wortmannin on PTX-induced Rac activation. Cells were pretreated with wortmannin (*WTM*; 100 nM) for 10 min before PTX stimulation. *C*, localization of GFP-fused wild type Rac and constitutively active Rac (*CA-Rac*) (G12V) with or without PTX stimulation. *D*, localization of GFP-fused PX domain of p40^{phox} (p40^{phox}-PX), and PI-3-P interaction-deficient mutant (p40^{phox}-PX (R105K)) with or without PTX treatment. *, $p < 0.05$ *versus* PTX-untreated cells. *Error bars*, S.E.

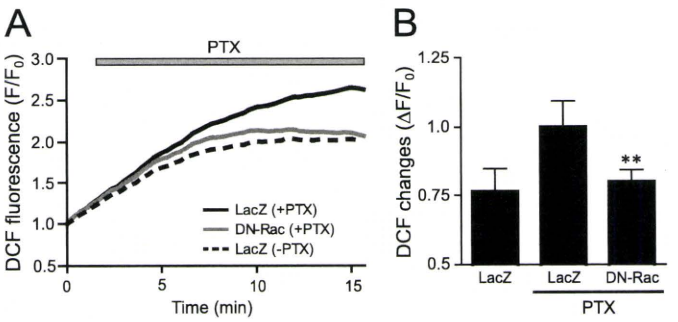

FIGURE 5. **Effects of DN-Rac on PTX-induced ROS production.** *A* and *B*, average changes (*A*) and peak increases (*B*) in PTX-induced F/F_0 of dichlorofluorescein from time course experiments. The increases in PTX-induced fluorescence of dichlorofluorescein were calculated by the value of maximal fluorescence intensity (*F*) during 20 min of stimulation and initial value of fluorescence, F_0. *, $p < 0.05$; **, $p < 0.01$ *versus* PTX-untreated or LacZ-expressing cells. *Error bars*, S.E.

PX, a specific marker for PI-3-P, was expressed (53). Under the basal condition, p40^{phox}-PX was predominantly localized in the PI-3-P-enriched early endosome and nucleus (Fig. 4*D*). Treatment with PTX for 10 min promoted the translocation of p40^{phox}-PX from early endosome to the plasma membrane. However, PTX did not affect the localization of p40^{phox}-PX (R105K), a mutant that cannot recognize PI-3-P. The localization of the PH domain of GRP1 (54), a marker for PI 3,4,5-trisphosphate, and that of the PH domain of PLCδ1, a marker for PI 4,5-bisphosphate, were not changed by PTX (data not shown). These results suggest that PTX-induced PI-3-P production through PI 3-kinase activation is required for translocation and activation of Rac.

Involvement of Rac in PTX-induced ROS Production—One of the targets for Rac is NADPH oxidase. Because the PTX-induced NF-κB activation was suppressed by DPI, DN-Rac, and DN-p47^{phox} (Fig. 3*F*), Rac-mediated activation of NADPH oxidase may participate in PTX-induced NF-κB activation. We found that PTX gradually increased dichlorofluorescein fluorescence intensity, indicating ROS production in cardiac fibroblasts (Fig. 5). The expression of DN-Rac completely sup-

pressed this ROS production, suggesting that PTX activates Rac and turns on a signaling cascade downstream of Rac.

Essential Role of Rac in PTX-induced AT1R Up-regulation—Because PTX-induced ROS production, NF-κB activation, and increase in AT1R density were inhibited by DN-Rac, Rac may play a central role in regulation of AT1R density. Inhibitors of 3-hydroxy-3-methylglutaryl-CoA reductase (statins) are known to suppress the activity of Rho family G proteins by inhibition of isoprenylation (55). It has been reported that simvastatin inhibits Rac activity in the H9c2 cell line and rat neonatal cardiomyocytes (56, 57). Simvastatin is also reported to reduce AT1R density in vascular smooth muscle cells (58). Therefore, we examined whether simvastatin inhibits IL-1β-induced up-regulation of AT1R by inhibition of Rac. Treatment with simvastatin completely suppressed the IL-1β-induced Rac activation (supplemental Fig. 4). Consistent with this result, the IL-1β-induced up-regulation of AT1R was also suppressed by simvastatin and DN-Rac. The Ang II-induced Ca^{2+} release was also enhanced in IL-1β-treated cells, and this enhancement was completely suppressed by simvastatin. These results suggest that simvastatin suppresses IL-1β-induced up-regulation of AT1R by inhibition of Rac activity. To prove the requirement of Rac in AT1R up-regulation more directly, we used Rac1 siRNAs. Knockdown of Rac1 almost completely suppressed IL-1β-induced Rac activation (Fig. 6*A*), increase in AT1R density (Fig. 6*B*), and enhancement of AT1R-stimulated Ca^{2+} responses (supplemental Fig. 4). Thus, Rac1 may predominantly regulate AT1R up-regulation by agonist stimulation. Because IL-1β induces Rac activation and PTX-induced IL-1β production was completely suppressed by knockdown of Rac1 (Fig. 6*C*), we hypothesize that PTX-induced IL-1β production plays a role in amplification of Rac activation. Treatment with IL-1β siRNA suppressed the PTX-induced Rac activation at a late phase of activation (from 6 h after the treatment) but did not suppress Rac activation at an early phase of activation (Fig. 6, *D* and *E*). Furthermore, IL-1β siRNA also suppressed PTX-induced nuclear localization of NF-κB in a late phase but not an early phase (Fig. 6, *F* and *G*). These results suggest that PTX-induced IL-1β production participates in the sustained activation of Rac and NF-κB, which is essential for AT1R up-regulation.

PTX Stimulates TLR4, Leading to Rac Activation—We next examined which receptor(s) functions as a target of PTX in cardiac fibroblasts. Because TLR4 is reported to work as a putative candidate receptor of B-oligomer (10), we examined whether stimulation of TLR4 is required for PTX-induced AT1R up-regulation in cardiac fibroblasts. Treatment with TLR4 siRNAs (si-88, si-1002, and si-1621) significantly decreased TLR4 mRNA levels but did not decrease AT1R mRNA levels (Fig. 7*A*). The PTX-induced enhancement of Ang II-induced Ca^{2+} release and increase in Rac activity were completely abolished by TLR4 siRNA treatment (Fig. 7, *B* and *C*). In contrast, PTX-induced ADP-ribosylation of $G\alpha_i$ proteins was not suppressed but preferably enhanced by TLR4 knockdown (Fig. 7*D*). These results suggest that TLR4 mediates PTX-induced Rac activation and AT1R up-regulation, but TLR4 does not mediate PTX-induced ADP-ribosylation of $G\alpha_i$ proteins.

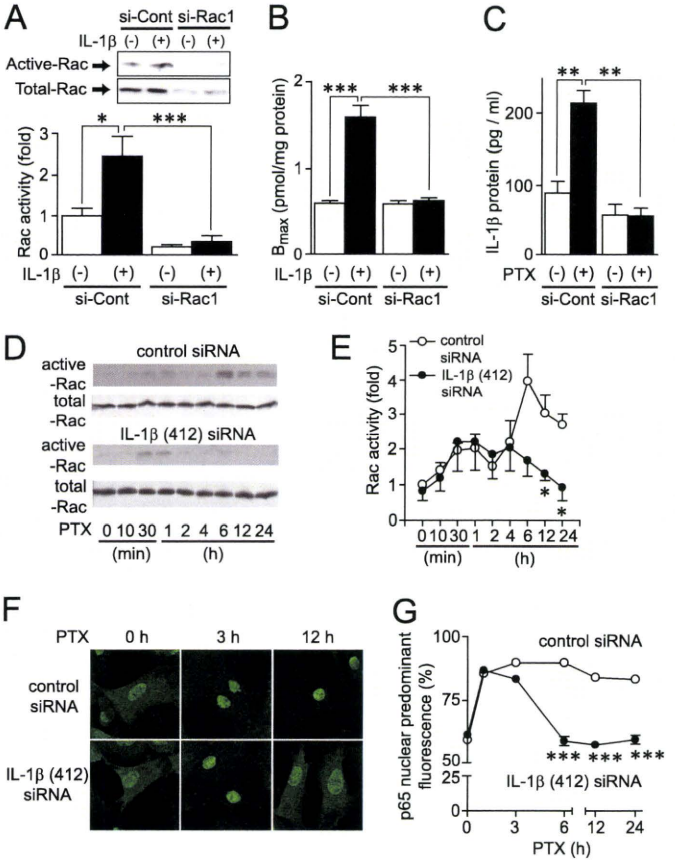

FIGURE 6. **Amplification of Rac-mediated signaling by PTX-induced IL-1β production.** *A*, cells were transfected with siRNAs for Rac1 (*si-Rac1*) or their randomized controls (*si-Cont*) for 72 h before 5-min stimulation with IL-1β (10 ng/ml). *B*, effects of si-Rac1 on the maximal increases in AT1R density by IL-1β stimulation. Cells were treated with IL-1β for 24 h before membrane preparation. *C*, effects of si-Rac1 on PTX-induced production of IL-1β proteins. Cells were treated with PTX (100 ng/ml) for 90 min. *D* and *E*, effects of IL-1β siRNA on PTX-induced Rac activation. Cells were transfected with IL-1β (412) siRNA (100 nM) for 48 h before treatment with PTX (100 ng/ml). *F* and *G*, effects of IL-1β (412) siRNA on PTX-induced nuclear localization of the NF-κB p65 subunit. More than 100 cells were scanned and quantified the subcellular localization of p65 using Photoshop (13, 27). *, $p < 0.05$; ***, $p < 0.001$ *versus* IL-1β-treated or control siRNA-treated cells. *Error bars*, S.E.

DISCUSSION

In this study, we demonstrated a novel action of PTX that enhances AT1R-stimulated Ca^{2+} response through AT1R up-regulation independently of ADP-ribosylation in rat cardiac fibroblasts. Using PTX as a powerful tool for analyzing the mechanism of AT1R up-regulation, we demonstrated that stimulation of TLR4 by PTX B-oligomer enhances AT1R function. Previous reports have suggested that Syk (spleen tyrosine kinase) and PI 3-kinase participate in TLR4-mediated responses (49, 59). We found that PTX-induced Rac activation was completely suppressed by inhibition of Syk (supplemental Fig. 3) and PI 3-kinase (Fig. 5), suggesting that Syk and PI 3-kinase mediate PTX-induced Rac activation. We also found that Rac-mediated NF-κB activation through ROS production plays a central role in the regulation of AT1R density. The PTX-induced NF-κB activation was suppressed by DPI and the dominant negative mutants of Rac and $p47^{phox}$ (Fig. 3). Because DPI is an inhibitor of NADPH oxidase and Rac and $p47^{phox}$ are essential compo-

nents of NADPH oxidase activation, the origin of PTX-induced ROS production may be NADPH oxidase. In addition, PTX induced degradation of IκBα proteins in a time-dependent manner, which was abolished by Rac inhibition (supplemental Fig. 3). Although molecular mechanism underlying ROS-mediated NF-κB activation is still unknown, this result implies that ROS-mediated inhibition of mitogen-activated protein kinase phosphatases may be involved (60). Because the promoter regions of IL-1β and AT1R contain a putative NF-κB binding site, AT1R up-regulation may be induced by direct interaction of AT1R promoter with NF-κB. However, PTX-induced enhancement of Ca^{2+} response by AT1R stimulation was almost completely suppressed by anti-IL-1β antibody and IL-1β siRNAs (Fig. 2). Thus, IL-1β released from fibroblasts by PTX treatment may be the main mechanism of PTX-induced AT1R up-regulation. Furthermore, Rac1 inhibition suppressed PTX-induced IL-1β production, and IL-1β inhibition suppressed PTX-induced Rac activation at a late but not an early phase (Fig. 6). Thus, Rac-mediated IL-1β production may amplify Rac-dependent signaling through IL-1β-mediated Rac activation. These results suggest that PTX induces AT1R up-regulation through a TLR4 → PI 3-kinase → Rac → NADPH oxidase → ROS → NF-κB → IL-1β-dependent signal pathway (Fig. 8).

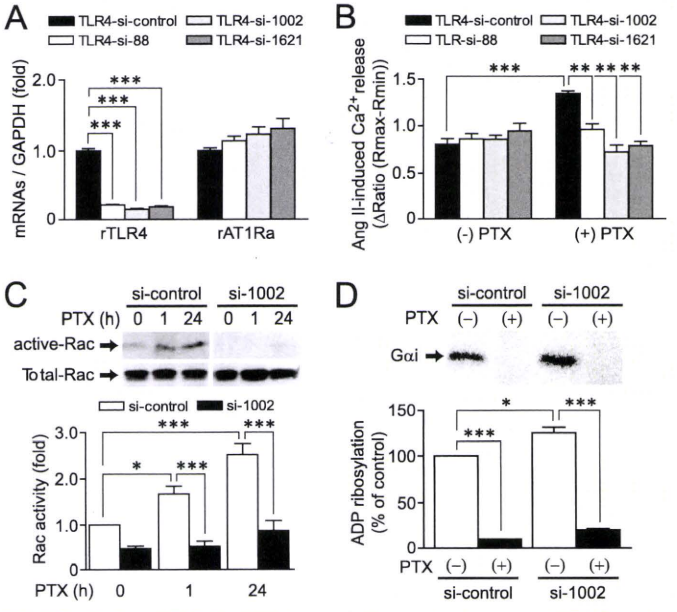

FIGURE 7. **Roles of TLR4 in PTX-induced Rac activation and ADP-ribosylation of G_i/G_o.** *A*, effects of TLR4 siRNAs on the expression of TLR4 and AT1R mRNAs. *B*, effects of TLR4 siRNAs on PTX-induced enhancement of Ang II-induced Ca^{2+} responses. Cells were treated with PTX for 24 h after siRNA treatment for 48 h. *C*, effects of TLR4 siRNA (si-1002) on PTX-induced Rac activation. *D*, effects of TLR4 siRNA on PTX-induced ADP-ribosylation of $G\alpha_i$ proteins. *, $p < 0.05$; **, $p < 0.01$; ***, $p < 0.001$. *Error bars*, S.E.

We revealed that stimulation of TLR4 mediates PTX-induced AT1R up-regulation. It is thought that MyD88 and Trif-related adaptor molecule mediate TLR4-mediated NF-κB activation (32). However, it has recently been reported that oxidized LDL induces NADPH oxidase-dependent ROS production through TLR4 stimulation in macrophages (59). These authors have also demonstrated that Syk but not MyD88 is responsible for TLR4-mediated ROS production. In addition, another study has shown that stimulation of TLR4 by PTX B-oligomer induces activation of MyD88-independent signaling pathways (10). Thus, PTX induces stimulation of TLR4 that preferentially activates the Syk-dependent Rac signaling pathway.

PTX is frequently used as a specific tool to examine the involvement of G_i in cellular signaling. Abolishment of TLR4 by siRNA did not affect PTX-mediated ADP-ribosylation of G_i and G_o (Fig. 7*D*). Thus, PTX binds to two receptors; one is TLR4 that activates Rac and another is the binding site that liberates the A-protomer into cells. So far, the G_i/G_o-independent signaling pathway is not usually considered when PTX is used *in vitro* and *in vivo*. Because PTX activates Rac in addition to ADP-ribosylation of G_i and G_o, it is no longer thought that PTX is a specific inhibitor of receptor-G_i signaling.

Another important finding of this study is that Rac is a physiological mediator of AT1R up-regulation induced by IL-1β stimulation. The inhibition of Rac suppressed the increase in AT1R density and the enhancement of Ang II-induced Ca^{2+} response by IL-1β stimulation (Fig. 6 and supplemental Fig. 4). Because other agonists that up-regulate AT1R, such as Ang II and TNF-α, also increase Rac activity, Rac-mediated AT1R up-regulation may be a common mechanism among various stimuli. Statins are inhibitors of 3-hydroxy-3-methylglutaryl-CoA reductase and appear

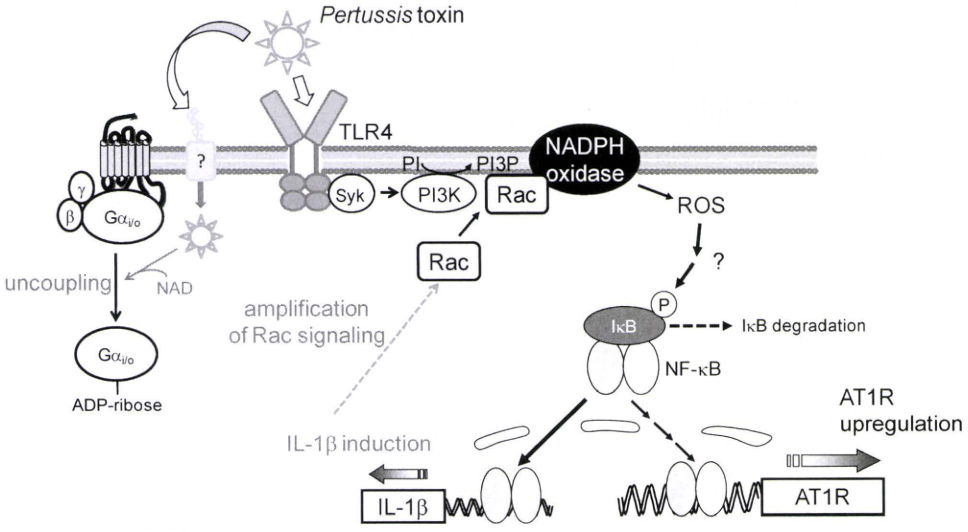

FIGURE 8. **Schema of TLR4-mediated AT1R up-regulation induced by PTX.** PTX induces ROS production through sequential activation of TLR4, Syk, PI 3-kinase (*PI3K*), Rac, and NADPH oxidase. Although the mechanism of NF-κB activation induced by ROS is still unknown, ROS mediate NF-κB-dependent expression of IL-1β. Induction of IL-1β also induces Rac activation through IL-1 receptor stimulation, leading to amplification of Rac-dependent signaling. Sustained activation of Rac may be required for PTX-induced AT1R up-regulation in rat cardiac fibroblasts. A-protomer of PTX enters the cells through unidentified binding site, and ADP-ribosylates G_i/G_o proteins.

to have pleiotropic effects on the cardiovascular system that are independent of their ability to decrease serum cholesterol (14, 55). These include inhibition of cardiac hypertrophy and left ventricular dysfunction, anti-inflammatory effects, and antioxidative effects (55, 61). Recent studies have demonstrated that statins inhibit ROS production and myocardial apoptosis by inhibition of Rac (57). Up-regulation of AT1R is thought to be one of the features involved in cardiac remodeling. Thus, the present results suggest a novel mechanism in which statins inhibit cardiac fibrosis by inhibition of AT1R up-regulation in cardiac fibroblasts. Statins also inhibit Rho activity by inhibition of isoprenylation. However, we could not detect the activation of Rho, Ras, and Rap1 by PTX treatment (supplemental Fig. 2). Thus, inhibition of Rac is essential for the inhibition of AT1R up-regulation by statin.

In conclusion, we demonstrated a novel action of PTX that induces AT1R up-regulation independently of ADP-ribosylation of G_i/G_o. This mechanism includes TLR4-mediated Rac activation, ROS production, and NF-κB activation. Activation of NF-κB induces IL-1β production, resulting in amplification of Rac signaling, which leads to increase in AT1R density. The involvement of the TLR4-Rac signaling pathway in the regulation of AT1R density will provide a possible novel target for inhibiting cardiac remodeling. In addition, we have provided pharmacologically important information indicating that PTX *per se* influences G protein-coupled receptor signaling independently of $G\alpha_i$ inhibition. Activation of the TLR4-Rac signaling pathway by PTX suggests that we should consider pharmacological actions of PTX in addition to a specific inhibitor of G_i/G_o-mediated signal transduction.

Acknowledgment—We thank Miyuki Toyotaka for analyzing the localization of the NF-κB p65 subunit.

REFERENCES

1. Katada, T., and Ui, M. (1982) *J. Biol. Chem.* **257,** 7210–7216
2. Kurose, H., Katada, T., Amano, T., and Ui, M. (1983) *J. Biol. Chem.* **258,** 4870–4875
3. Tamura, M., Nogimori, K., Yajima, M., Ase, K., and Ui, M. (1983) *J. Biol. Chem.* **258,** 6756–6761
4. Lando, Z., Teitelbaum, D., and Arnon, R. (1980) *Nature* **287,** 551–552
5. Linthicum, D. S., Munoz, J. J., and Blaskett, A. (1982) *Cell Immunol.* **73,** 299–310
6. Racke, M. K., Hu, W., and Lovett-Racke, A. E. (2005) *Trends Immunol.* **26,** 289–291
7. Jajoo, S., Mukherjea, D., Pingle, S., Sekino, Y., and Ramkumar, V. (2006) *J. Pharmacol. Exp. Ther.* **317,** 1–10
8. Li, H., and Wong, W. S. (2001) *Biochem. Biophys. Res. Commun.* **283,** 1077–1082
9. Melien, O., Sandnes, D., Johansen, E. J., and Christoffersen, T. (2000) *J. Cell Physiol.* **184,** 27–36
10. Wang, Z. Y., Yang, D., Chen, Q., Leifer, C. A., Segal, D. M., Su, S. B., Caspi, R. R., Howard, Z. O., and Oppenheim, J. J. (2006) *Exp. Hematol.* **34,** 1115–1124
11. Timmermans, P. B., Wong, P. C., Chiu, A. T., Herblin, W. F., Benfield, P., Carini, D. J., Lee, R. J., Wexler, R. R., Saye, J. A., and Smith, R. D. (1993) *Pharmacol. Rev.* **45,** 205–251
12. de Gasparo, M., Catt, K. J., Inagami, T., Wright, J. W., and Unger, T. (2000) *Pharmacol. Rev.* **52,** 415–472
13. Onohara, N., Nishida, M., Inoue, R., Kobayashi, H., Sumimoto, H., Sato, Y., Mori, Y., Nagao, T., and Kurose, H. (2006) *EMBO J.* **25,** 5305–5316
14. Brown, R. D., Ambler, S. K., Mitchell, M. D., and Long, C. S. (2005) *Annu. Rev. Pharmacol. Toxicol.* **45,** 657–687
15. Villarreal, F. J., Kim, N. N., Ungab, G. D., Printz, M. P., and Dillmann, W. H. (1993) *Circulation* **88,** 2849–2861
16. Sakata, Y., Hoit, B. D., Liggett, S. B., Walsh, R. A., and Dorn, G. W., 2nd (1998) *Circulation* **97,** 1488–1495
17. Gurantz, D., Cowling, R. T., Varki, N., Frikovsky, E., Moore, C. D., and Greenberg, B. H. (2005) *J. Mol. Cell Cardiol.* **38,** 505–515
18. Nio, Y., Matsubara, H., Murasawa, S., Kanasaki, M., and Inada, M. (1995) *J. Clin. Invest.* **95,** 46–54
19. Yamani, M. H., Cook, D. J., Tuzcu, E. M., Abdo, A., Paul, P., Ratliff, N. B., Yu, Y., Yousufuddin, M., Feng, J., Hobbs, R., Rincon, G., Bott-Silverman, C., McCarthy, P. M., Young, J. B., and Starling, R. C. (2004) *Am. J. Transplant.* **4,** 1097–1102
20. Peng, J., Gurantz, D., Tran, V., Cowling, R. T., and Greenberg, B. H. (2002) *Circ. Res.* **91,** 1119–1126
21. Finkel, T. (1999) *J. Leukoc. Biol.* **65,** 337–340
22. Griendling, K. K., and Ushio-Fukai, M. (2000) *Regul. Pept.* **91,** 21–27
23. Sundaresan, M., Yu, Z. X., Ferrans, V. J., Sulciner, D. J., Gutkind, J. S., Irani, K., Goldschmidt-Clermont, P. J., and Finkel, T. (1996) *Biochem. J.* **318,** 379–382
24. Sumimoto, H. (2008) *FEBS J.* **275,** 3249–3277
25. Sulciner, D. J., Irani, K., Yu, Z. X., Ferrans, V. J., Goldschmidt-Clermont, P., and Finkel, T. (1996) *Mol. Cell Biol.* **16,** 7115–7121
26. Nishida, M., Tanabe, S., Maruyama, Y., Mangmool, S., Urayama, K., Nagamatsu, Y., Takagahara, S., Turner, J. H., Kozasa, T., Kobayashi, H., Sato, Y., Kawanishi, T., Inoue, R., Nagao, T., and Kurose, H. (2005) *J. Biol. Chem.* **280,** 18434–18441
27. Fujii, T., Onohara, N., Maruyama, Y., Tanabe, S., Kobayashi, H., Fukutomi, M., Nagamatsu, Y., Nishihara, N., Inoue, R., Sumimoto, H., Shibasaki, F., Nagao, T., Nishida, M., and Kurose, H. (2005) *J. Biol. Chem.* **280,** 23041–23047
28. Pracyk, J. B., Tanaka, K., Hegland, D. D., Kim, K. S., Sethi, R., Rovira, I. I., Blazina, D. R., Lee, L., Bruder, J. T., Kovesdi, I., Goldshmidt-Clermont, P. J., Irani, K., and Finkel, T. (1998) *J. Clin. Invest.* **102,** 929–937
29. Sussman, M. A., Welch, S., Walker, A., Klevitsky, R., Hewett, T. E., Price, R. L., Schaefer, E., and Yager, K. (2000) *J. Clin. Invest.* **105,** 875–886
30. Ichiki, T., Takeda, K., Tokunou, T., Iino, N., Egashira, K., Shimokawa, H., Hirano, K., Kanaide, H., and Takeshita, A. (2001) *Arterioscler. Thromb. Vasc. Biol.* **21,** 1896–1901
31. Akira, S., Uematsu, S., and Takeuchi, O. (2006) *Cell* **124,** 783–801
32. Chao, W. (2009) *Am. J. Physiol. Heart Circ. Physiol.* **296,** H1–H12
33. Kurose, H., Arriza, J. L., and Lefkowitz, R. J. (1993) *Mol. Pharmacol.* **43,** 444–450
34. Nishida, M., Sato, Y., Uemura, A., Narita, Y., Tozaki-Saitoh, H., Nakaya, M., Ide, T., Suzuki, K., Inoue, K., Nagao, T., and Kurose, H. (2008) *EMBO J.* **27,** 3104–3115
35. Nishida, M., Sugimoto, K., Hara, Y., Mori, E., Morii, T., Kurosaki, T., and Mori, Y. (2003) *EMBO J.* **22,** 4677–4688
36. Nagamatsu, Y., Nishida, M., Onohara, N., Fukutomi, M., Maruyama, Y., Kobayashi, H., Sato, Y., and Kurose, H. (2006) *J. Pharmacol. Sci.* **101,** 144–150
37. Chiloeches, A., Paterson, H. F., Marais, R., Clerk, A., Marshall, C. J., and Sugden, P. H. (1999) *J. Biol. Chem.* **274,** 19762–19770
38. Franke, B., Akkerman, J. W., and Bos, J. L. (1997) *EMBO J.* **16,** 252–259
39. Arai, K., Maruyama, Y., Nishida, M., Tanabe, S., Takagahara, S., Kozasa, T., Mori, Y., Nagao, T., and Kurose, H. (2003) *Mol. Pharmacol.* **63,** 478–488
40. Ju, H., Zhao, S., Tappia, P. S., Panagia, V., and Dixon, I. M. (1998) *Circulation* **97,** 892–899
41. Bai, H., Wu, L. L., Xing, D. Q., Liu, J., and Zhao, Y. L. (2004) *Chin. Med. J.* **117,** 88–93
42. He, J., Gurunathan, S., Iwasaki, A., Ash-Shaheed, B., and Kelsall, B. L. (2000) *J. Exp. Med.* **191,** 1605–1610
43. Maruyama, Y., Nishida, M., Sugimoto, Y., Tanabe, S., Turner, J. H., Kozasa, T., Wada, T., Nagao, T., and Kurose, H. (2002) *Circ. Res.* **91,** 961–969
44. Nishida, M., Maruyama, Y., Tanaka, R., Kontani, K., Nagao, T., and Kurose, H. (2000) *Nature* **408,** 492–495